The STAGGER-grid: A grid of 3D stellar atmosphere models

A. Chiavassa, L. Casagrande, R. Collet, Z. Magic, L. Bigot, Frédéric Thévenin, M. Asplund

A&A 611, A11 (2018)
https://doi.org/10.1051/0004-6361/201732147

Astronomy & Astrophysics

The STAGGER-grid: A grid of 3D stellar atmosphere models

V. Synthetic stellar spectra and broad-band photometry⋆

A. Chiavassa[1], L. Casagrande[2], R. Collet[3], Z. Magic[4,5], L. Bigot[1], F. Thévenin[1], and M. Asplund[2]

[1] Université Côte d'Azur, Observatoire de la Côte d'Azur, CNRS, Lagrange, CS 34229, 06300 Nice, France
e-mail: andrea.chiavassa@oca.eu
[2] Research School of Astronomy & Astrophysics, Australian National University, Cotter Road, Weston, ACT 2611, Australia
[3] Stellar Astrophysics Centre, Department of Physics and Astronomy, Aarhus University, Ny Munkegade 120, 8000 Aarhus C, Denmark
[4] Niels Bohr Institute, University of Copenhagen, Juliane Maries Vej 30, 2100 Copenhagen, Denmark
[5] Centre for Star and Planet Formation, Natural History Museum of Denmark, University of Copenhagen, Øster Voldgade 5-7, 1350 Copenhagen, Denmark

Received 20 October 2017 / Accepted 4 January 2018

ABSTRACT

Context. The surface structures and dynamics of cool stars are characterised by the presence of convective motions and turbulent flows which shape the emergent spectrum.
Aims. We used realistic three-dimensional (3D) radiative hydrodynamical simulations from the STAGGER-grid to calculate synthetic spectra with the radiative transfer code OPTIM3D for stars with different stellar parameters to predict photometric colours and convective velocity shifts.
Methods. We calculated spectra from 1000 to 200 000 Å with a constant resolving power of $\lambda/\Delta\lambda = 20\,000$ and from 8470 and 8710 Å (*Gaia* Radial Velocity Spectrometer – RVS – spectral range) with a constant resolving power of $\lambda/\Delta\lambda = 300\,000$.
Results. We used synthetic spectra to compute theoretical colours in the Johnson-Cousins $UBV(RI)_C$, SDSS, 2MASS, *Gaia*, SkyMapper, Strömgren systems, and HST-WFC3. Our synthetic magnitudes are compared with those obtained using 1D hydrostatic models. We showed that 1D versus 3D differences are limited to a small percent except for the narrow filters that span the optical and UV region of the spectrum. In addition, we derived the effect of the convective velocity fields on selected Fe I lines. We found the overall convective shift for 3D simulations with respect to the reference 1D hydrostatic models, revealing line shifts of between −0.235 and +0.361 km s^{-1}. We showed a net correlation of the convective shifts with the effective temperature: lower effective temperatures denote redshifts and higher effective temperatures denote blueshifts. We conclude that the extraction of accurate radial velocities from RVS spectra need an appropriate wavelength correction from convection shifts.
Conclusions. The use of realistic 3D hydrodynamical stellar atmosphere simulations has a small but significant impact on the predicted photometry compared with classical 1D hydrostatic models for late-type stars. We make all the spectra publicly available for the community through the POLLUX database.

Key words. stars: atmospheres – stars: fundamental parameters – techniques: photometric – techniques: radial velocities – hydrodynamics – radiative transfer

1. Introduction

The stellar atmosphere is the boundary to the opaque stellar interior, and serves as the link between observations and the models of stellar structure and evolution. The phenomena of stellar evolution manifest themselves in the stellar surface as changes in chemical composition and in fundamental stellar parameters such as radius, surface gravity, effective temperature, and luminosity. The information we use to study distant stars comes from the flux they have emitted. However, the atmospheric layers where this flux forms is the transition region between convective and radiative regime. Thus, the surface structures and dynamics of cool stars are characterised by the presence of convective motions and turbulent flows. Convection manifests in the surface layers as a particular pattern of downflowing cooler plasma and bright areas where hot plasma rises (Nordlund et al. 2009). The size of granules depends on the stellar parameters of the star and, as a consequence, on the extension of their atmosphere (e.g. Magic et al. 2013). Eventually, the convection causes an inhomogeneous stellar surface that changes with time. They affect the atmospheric stratification in the region where the flux forms and also affect the emergent spectral energy distribution (SED), with potential effects on the precise determinations of stellar parameters (e.g. Bigot et al. 2011; Creevey et al. 2012; Chiavassa et al. 2012), radial velocity (e.g. Bigot & Thévenin 2008; Chiavassa et al. 2011; Allende Prieto et al. 2013), chemical abundance (e.g. Asplund et al. 2005, 2009; Caffau et al. 2011), photometric colours (Bonifacio et al. 2017), and on planet detection (Magic et al. 2015; Chiavassa et al. 2017).

Convection is a difficult process to understand because it is non-local, and 3D, and it involves non-linear interactions over many disparate length scales. In this context, the use of numerical 3D radiative hydrodynamical simulations of stellar convection is extremely important. In recent years, with

⋆ Tables 5–8 are only available at the CDS and Table B.1 is also available at the CDS and via anonymous ftp to cdsarc.u-strasbg.fr (130.79.128.5) or via http://cdsarc.u-strasbg.fr/viz-bin/qcat?J/A+A/611/A11

increased computational power, it has been possible to compute grids of 3D simulations that cover a substantial portion of the Hertzsprung–Russell diagram (Magic et al. 2013; Trampedach et al. 2013; Ludwig et al. 2009). With these tools it is possible to predict reliable synthetic spectra for several stellar types.

Photometric systems and filters are designed to be sensitive to temperature, gravity, and metal abundance indicators and thereby to complement spectroscopic determinations of the fundamental properties of stars. In addition, the integrated magnitudes and colours of stars can be used to infer the ages, metallicities, and other properties of the underlying stellar populations (e.g. Casagrande & VandenBerg 2014). For these purposes, several broad-band, or intermediate- and/or narrow-band filters have been designed to probe different regions of stellar spectra sensitive to different atmospheric parameters (Bessell & Murphy 2012; Gunn et al. 2006; Cohen et al. 2003). Additionally, there are the photometric systems used by the *Gaia* mission.

Gaia (Gaia Collaboration 2016) is an astrometric, photometric, and spectroscopic spaceborne mission of a large part of the Milky Way. Apart from the astrometric instrument, *Gaia* carries on board two low-resolution spectrophotometers (Blue and Red Prism, BP/RP, Bailer-Jones et al. 2013) and the Radial Velocity Spectrometer (RVS; Katz et al. 2004). The photometric instrument measures the SED over 120 pixels of all detected objects at the same angular resolution and at the same epoch as the astrometric observations. The BP operates in the range 3300–6800 Å, while the RP uses the range 6400–10 500 Å. The main aims of this instrument are to provide proper classifications (e.g. distinguish between stars, galaxies, and quasars) and characterisations (e.g. reddenings and stellar parameters), and to enable chromatic corrections of the astrometric centroid data. Finally, the integral-field spectrograph RVS provides spectra between 8470 and 8710 Å at a spectral resolving power of ≈11 200. The RVS is expected to produce radial velocities through Doppler-shift measurements; interstellar reddening, atmospheric parameters, and projected rotational velocities; and individual element abundances for some elements.

In this work, we calculated synthetic stellar spectra and photometry for broad-band and *Gaia* systems obtained using realistic 3D radiative hydrodynamical simulations of stellar convection from the STAGGER-grid. The predicted photometric 3D colours and the 3D spectra are publicly available for the community through the POLLUX database. The spectra corresponding to the *Gaia* RVS spectral range will be used for the calibration of the instrument to preserve the measured radial velocities from the convection shift (see forthcoming paper of GaiaDataRelease2/RVS).

2. Methods

2.1. Stellar model atmospheres

Magic et al. (2013) described the STAGGER-grid of realistic 3D radiative hydrodynamical simulations of stellar convection for cool stars using the STAGGER-code (originally developed by Nordlund & Galsgaard[1], and continuously improved over the years by its user community), a state-of-the-art (magneto)hydrodynamic code that solves the time-dependent hydrodynamic equations for mass-, momentum-, and energy-conservation, coupled with the 3D radiative transfer equation in order to account correctly for the interaction between the radiation field and the plasma. The code uses periodic boundary conditions horizontally and open boundaries vertically. At the bottom of the simulation, the inflows have a constant entropy. The outflows are not tightly constrained and are free to pass through the boundary. The code is based on a sixth-order explicit finite-difference scheme and a fifth-order interpolation. The considered large number over wavelength points is merged into 12 opacity bins (Nordlund 1982; Skartlien 2000; Magic et al. 2013). STAGGER simulations are based on a realistic equation of state that accounts for ionisation, recombination, and dissociation (Mihalas et al. 1988); continuous absorption and scattering coefficients listed in Hayek et al. (2010); and the line opacities listed in Gustafsson et al. (2008). These are in turn based on the VALD-2 database (Stempels et al. 2001) of atomic lines and the SCAN-base (Jørgensen 1997) of molecular lines.

2.2. Three-dimensional radiative transfer

We used the 3D pure-LTE radiative transfer code OPTIM3D (Chiavassa et al. 2009) to compute synthetic spectrum from the snapshots of the radiative-hydrodynamical (RHD) simulations of the STAGGER-grid (see Fig. 1 in Magic et al. 2013). The code takes into account the Doppler shifts due to convective motions. The radiative transfer equation is solved monochromatically using pre-tabulated extinction coefficients as a function of temperature, density, and wavelength.
The lookup tables were computed for the same chemical compositions as the RHD simulations using the same extensive atomic and molecular continuum and line opacity data as the latest generation of MARCS models (Gustafsson et al. 2008) with the addition – with respect to Table 2 of Gustafsson's paper – of the SiS molecule (Cami et al. 2009), which is particularly important for the far-infrared region of the spectrum. While the sources of line opacities used in the RHD simulations of Magic et al. (2013) and in OPTIM3D are the same, the data for the continuum opacities are almost the same: Hayek et al. (2010) reported that the data used in RHD simulations are mostly identical to those used in the MARCS models, but include additional bound-free data from the Opacity Project and the Iron Project (Trampedach et al., priv. comm.) as well as some opacities of the second ionisation stage for many metals.

For the computation of the spectra from RHD simulations, the assumed microturbulence is equal to zero since the velocity fields inherent in RHD models are expected to self-consistently and adequately account for non-thermal Doppler broadening of spectral lines (Asplund 2000). The temperature and density ranges spanned by the tables are optimised for the values encountered in the RHD simulations. The detailed methods used in the code are explained in Chiavassa et al. (2009, 2010). OPTIM3D has already been employed in synergy with the STAGGER simulations in several works (Chiavassa et al. 2010, 2011, 2012, 2014a, 2015, 2017; Magic et al. 2015) either concerning the extraction of synthetic spectra or interferometric observables.

2.3. One-dimensional radiative transfer

For all the following comparisons with 3D simulations, we used plane-parallel, hydrostatic, 1D atmosphere models computed with a similar physical treatment to the MARCS code and the same equation of state and opacities as in the individual 3D simulations (ATMO; Magic et al. 2013). Moreover, we used a 1D version of OPTIM3D, and the chemical compositions, the opacities, and numerics of the radiative transfer calculations for the emergent intensities are the same as used in the 1D and 3D approaches.

[1] http://www.astro.ku.dk/~kg/Papers/MHDcode.ps.gz

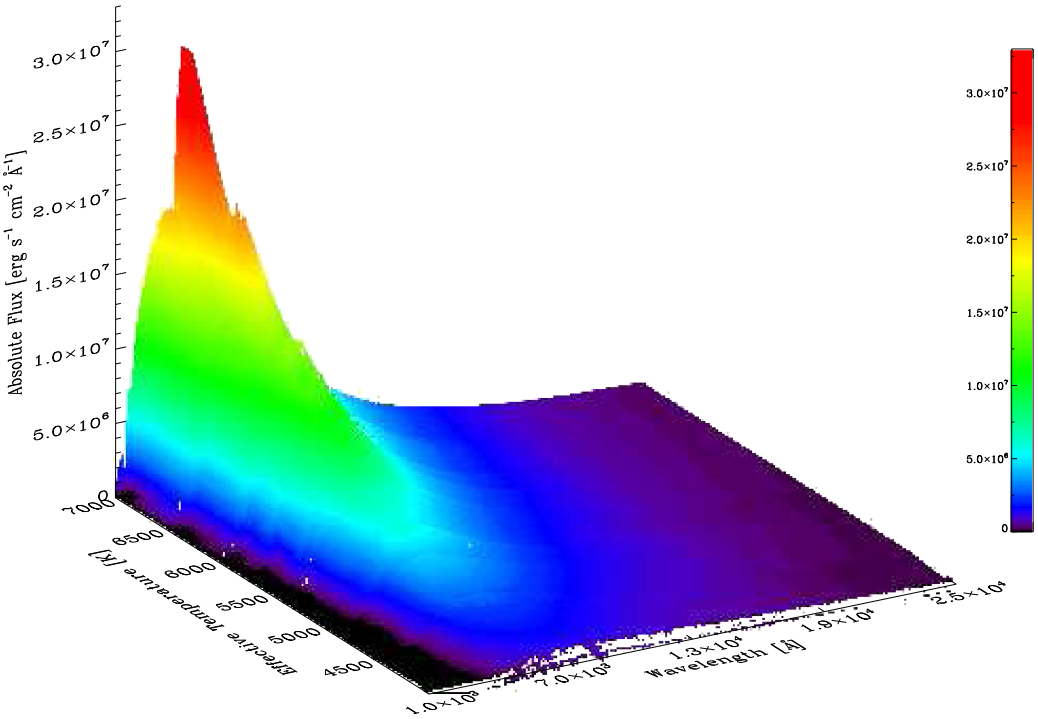

Fig. 1. Surface rendering for all the synthetic spectra computed for the 3D RHD simulations in Table B.1. The vertical bar on the right displays the colour scale for the emerging flux in erg s^{-1} cm^{-2} Å^{-1}. For clarity, the wavelength range has been reduced to 1000–25 000 Å.

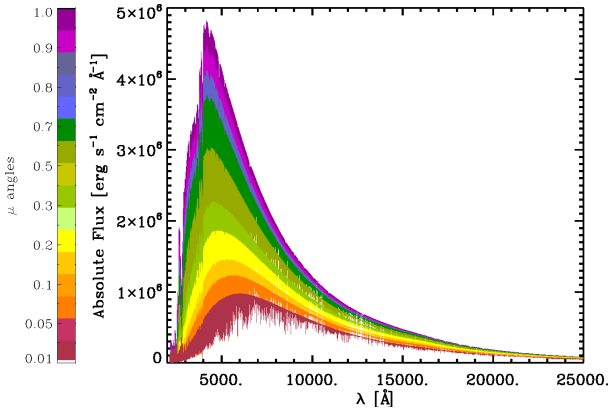

Fig. 2. Synthetic spectra of the solar simulation in the spectral range 2000–25 000 Å and for the different $\mu = \cos(\theta)$ inclination angles used in the computation, where θ is the angle with respect to the line of sight (vertical axis).

3. Synthetic spectra from 0.1 to 20 μm

The STAGGER-grid includes 3D stellar atmosphere simulations with metallicities [Fe/H] $= +0.5$, 0.0, -0.5, -1.0, -2.0, -3.0, and -4.0; surface gravity $\log g$ between 1.5 and 5.0 in steps of 0.5 dex; and effective temperature $T_{\rm eff}$ from 4000 to 7000 K in steps of 500 K (Fig. 1 of Paper I). In this work we present the synthetic spectra computed for the STAGGER-grid for a total of 181 simulations (Table B.1). The spectra have been calculated with a constant resolving power of $\lambda/\Delta\lambda = 20\,000$ ($n_\lambda = 105\,767$ wavelength points) from 1000 to 200 000 Å. OPTIM3D computes the emerging intensities for vertical rays cast through the computational box for all required wavelengths. The procedure is repeated after tilting the computational box by an angle θ with respect to the line of sight (vertical axis) and rotating it azimuthally by an angle ϕ. The final result is a spatially resolved intensity spectrum at different angles. In addition, a temporal average is also performed. We performed the calculations for ten snapshots of the 3D RHD simulations of Table B.1, adequately spaced so as to capture several convective turnovers, for ten different inclination angles $\mu = \cos(\theta) = [1.00, 0.90, 0.80, 0.70, 0.50, 0.30, 0.20, 0.10, 0.05, 0.01]$ (see Fig. 4), and four ϕ-angles [0°, 90°, 180°, 270°]. The strongest decline in the limb darkening is usually found towards the limb; therefore, we decided to resolve with more μ-angles at the limb instead of having an equidistant scale in μ. We tested the discrepancy between the temporal average using a large number of snapshots (e.g. 20) and using only 10 snapshots is lower than 0.3%. The number of ten snapshots was chosen because it represents the best compromise in terms of computational time and accuracy among the whole set of stellar parameters. All things considered, we computed 400 spectra in the range 1000–200 000 Å for every simulation.

Figure 1 displays the set of all synthetic spectra computed. We determined the $T_{\rm eff}$ from the integration of the SED of the spectra from 0.1 to 20 μm. The effective temperature has been computed using Stefan–Boltzmann law as

$$T_{\rm eff\ spectra} = \left\{ \left[\int_{\lambda_1}^{\lambda_2} f(\lambda)\, {\rm d}\lambda \right] / \sigma \right\}^{0.25}, \quad (1)$$

where $\lambda_1 = 1010$Å and $\lambda_2 = 199\,960$ Å, $f(\lambda)$ is the synthetic flux, and σ is the Stefan–Boltzmann constant. The values of the effective temperature are listed in Table B.1.

Figure 1 shows that increasing $T_{\rm eff}$ returns higher radiated energy per surface area and the peak of the radiation curve moves to shorter wavelengths, as expected by Planck law. Pereira et al. (2013) provided excellent agreement of their 3D solar simulation of the STAGGER-grid with the continuum observation of the Sun. As they did, we used the Kurucz (2005) irradiance[2] and normalised flux atlases for the Sun between 3000 and 10 000 Å and found a good agreement (Fig. 3), reinforcing the view that the simulation of thermodynamic structure

[2] Available at http://kurucz.harvard.edu/sun.html

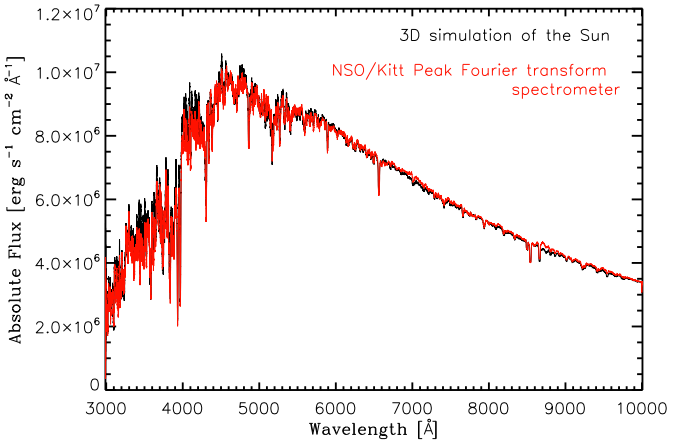

Fig. 3. Comparison of the solar simulation (black) with the observed flux of the Sun (red, Kurucz 2005). The solar irradiance is converted to flux at the solar surface using the multiplicative factor of $[(1\mathrm{AU})/R_\odot]^2 = 46\,202$. For clarity, the spectra have been resampled to a lower spectral resolution with fewer frequency points ($n_\lambda = 2115$).

Table 1. Photometric systems used in this work and overplotted on the synthetic spectra in Fig. 4.

Photometric system name	Filters
Johnson-Cousins[a]	$UBV(RI)_C$
Sloan Digital Sky Survey (SDSS)[b]	*ugriz*
2MASS[c]	J, H, K_S
Gaia[d]	G, BP, RP
SkyMapper[e]	$u_s, v_s, g_s, r_s, i_s, z_s$
Strömgren[f]	*uvby*
HST-WFC3[g]	*F*218*W*, *F*225*W*, *F*275*W*, *F*336*W*, *F*350*W*, *F*390*M*, *F*390*W*, *F*438*W*, *F*475*W*, *F*547*M*, *F*555*W*, *F*606*W*, *F*625*W*, *F*775*W*, *F*814*W*, *F*850*LP*

References. [(a)] Bessell & Murphy (2012), [(b)] Doi et al. (2010), [(c)] Cohen et al. (2003), [(d)] Jordi et al. (2010), [(e)] Bessell et al. (2011), [(f)] Bessell (2011), [(g)] Deustua et al. (2016).

and post-processing detailed radiative transfer are realistic. This conclusion was also reported by Hayek et al. (2012), who determined that the numerical resolution of the STAGGER 3D RHD models and the spectral resolution for the flux computations are sufficient to predict realistic observables. In particular, some of the RHD simulations presented in this work and for a limited spectral region between 2000 and 10 000 Å have been used in Magic et al. (2015) to provide appropriate coefficients for various bi-parametric and non-linear limb darkening laws.

4. Photometric synthetic observables

Photometric systems and filters are designed to probe fundamental physical parameters, such as the effective temperature, surface gravity, and metallicity of stars. Colour and magnitude relations are used for a variety of purposes: interpreting the observed distribution of stars in colour–colour and colour–magnitude diagrams, deriving distances to stars and star clusters, and testing stellar evolutionary theory by comparing with observations to name just a few. Thus, it is important to have realistic model fluxes to generate colours which match the observed values. In addition to synthetic model fluxes, details on the photometric standardisation are also a part of this quest.

In essence, photometry condenses the information encoded in a spectrum $f(\lambda)$ over a system response function $T(\lambda)$, i.e. $\int f(\lambda)\,T(\lambda)\,\mathrm{d}\lambda$. Each existing photometric system then varies in the details. Most notably, $T(\lambda)$ will depend on the filter under consideration and the response function of the detector. This means that a distinction must be made between photo-counting and energy-integration detectors, meaning that a measurement of energy $\int f(\lambda)\,T(\lambda)\,\mathrm{d}\lambda$ will correspond to $(hc)^{-1}\int f(\lambda)\,\lambda T(\lambda)\,\mathrm{d}\lambda$ photons (see e.g. Bessell 2000). Another aspect that often varies among different photometric systems is how their standardisation (zero-point and absolute calibration) is achieved. Here, for all systems but *Gaia* we adopted the exact same procedure as used by Casagrande & VandenBerg (2014), where details on the adopted filter transmission curves, the photo-counting and energy-integration formalism, and zero-points and absolute calibration can be found[3]. We computed synthetic colours in the Johnson-Cousins, SDSS, 2MASS, *Gaia*, SkyMapper, Strömgren, HST-WFC3, and *Gaia* systems (Table 1 and Fig. 4 for a comparison of the solar spectrum with the filter transmission curves studied here). For the HST-WFC3 systems our tables are provided in the VEGA, ST, and AB systems.

A full characterisation of the *Gaia* photometric system, including zero-points and standardisation is expected to be released in 2018. In this work, we used the transmission curves available from the ESA website[4], and computed *Gaia* colours following Jordi et al. (2010). We fixed Vega's magnitudes to be G = BP = RP = 0.03, and for the absolute calibration used a Kurucz synthetic Vega spectrum rescaled to the measured flux value at 5556 Å from Megessier (1995).

Similarly to Casagrande & VandenBerg (2014), instead of colour indices we provide bolometric corrections in different bands (Table B.1 and 4–7, available at the CDS) because they are more versatile and can be rearranged in any colour combination, as follows from Eqs. (3) and (4). The bolometric magnitude is defined as

$$M_{\mathrm{Bol}} = -2.5\log\frac{L}{L_\odot} + M_{\mathrm{Bol},\odot}, \tag{2}$$

where we adopt $M_{\mathrm{Bol},\odot} = 4.74$. It follows that the bolometric correction in a given band BC_ζ is

$$BC_\zeta = m_{\mathrm{Bol}} - m_\zeta = M_{\mathrm{Bol}} - M_\zeta, \tag{3}$$

where the lower and upper cases refer to apparent and absolute magnitudes, respectively. From this it follows that colour indices can be obtained from the difference in bolometric corrections, where ζ and η are two given bands:

$$\zeta - \eta = m_\zeta - m_\eta = BC_\eta - BC_\zeta. \tag{4}$$

Thus, in the rest of the paper when we talk about synthetic colours, these have been obtained as differences in bolometric corrections from our tables.

[3] The only difference with respect to Casagrande & VandenBerg (2014) is that here we have adopted $M_{\mathrm{Bol}\odot} = 4.74$.

[4] https://www.cosmos.esa.int/web/gaia/transmissionwithoriginal

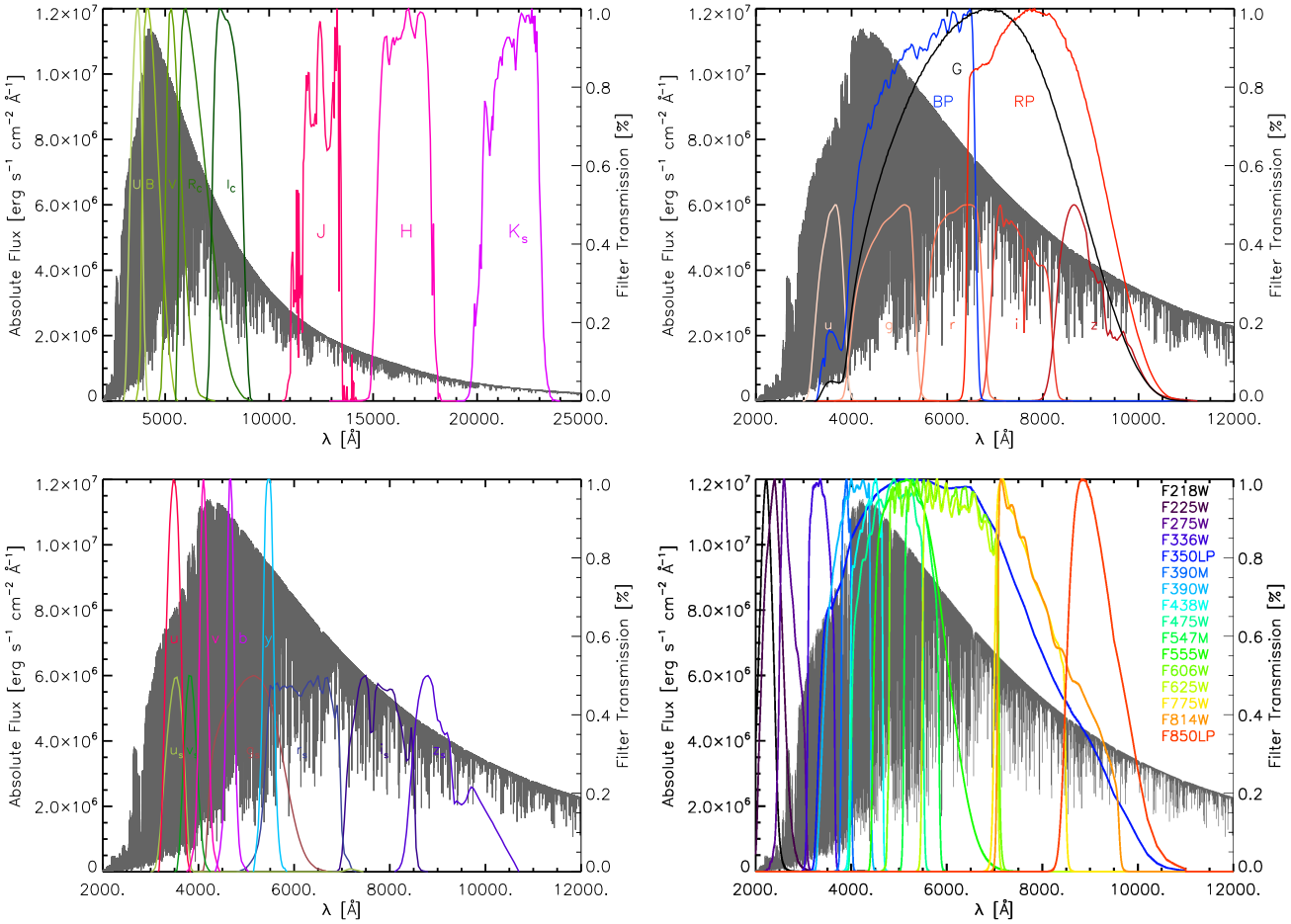

Fig. 4. Synthetic spectrum of the solar simulation at full spectral resolution in the spectral range 2000–25 000 Å (grey, *top panel*) and 2000–12 000 Å (*central* and *bottom* panels). Several system response functions (Table 1), from which synthetic colours have been computed, are overplotted. Johnson-Cousins system response functions (U, B, V, Rc, Ic) are plotted in green and 2MASS in pink-violet (*top left panel*); SDSS (u, g, r, i, z) in yellow-red and *Gaia* (BP, RP, G) (*top right panel*); Strömgren ($uvby$) in red-blue and SkyMapper ($u_s, v_s, g_s, r_s, i_s, z_s$) (*bottom left panel*); and the 15 filters of the HST-WFC3 (*bottom right panel*). For clarity, SDSS and SkyMapper functions are normalised to 0.5.

4.1. Microturbulence

The stellar surface convection produces a velocity field where the emerging spectral lines form. The Doppler broadening of these lines is a direct consequence of the velocity field in these crucial layers (Asplund et al. 2000b; Nordlund et al. 2009). In traditional 1D models, this effect can be accounted for by the use of arbitrary micro- and macroturbulence parameters. Full 3D line formation calculations using 3D RHD simulations have demonstrated that in late-type stars the required non-thermal Doppler line broadening is fully included in the convection-related motions of the stellar atmosphere (e.g. Collet et al. 2007). One-dimensional microturbulence represents the small-scale end of turbulent motions and is applied to the spectral line absorption coefficient. It affects the strong lines to a greater extent, reducing their saturation, and to a lesser extent the widths of weak lines. For 1D-based SEDs, microturbulence partly redistributes the flux in spectral regions probed by the photometric systems, in particular in regions crowded with lines towards the blue and the ultraviolet, and in filters with smaller wavelength coverages (Casagrande & VandenBerg 2014).

The values of the microturbulence parameters are usually determined by comparing synthetic and observed spectral line profiles and line strengths and often using a depth-independent value. For reference, a typical value for dwarfs and subgiants is around 1−1.5 km s^{-1}, which increases to 2−2.5 km s^{-1} for stars on the red giant branch (e.g. Gray et al. 2001). A constant value of 2 km s^{-1} is usually assumed in large grids of synthetic stellar spectra (Castelli & Kurucz 2004; Brott & Hauschildt 2005). To compute our 1D hydrostatic comparison models, we explored different values of microturbulence: 0, 1, and 2 km s^{-1}. We found that there is no clear and no unique relation between microturbulence and the stellar parameters, as reported by Casagrande & VandenBerg (2014). For clarity we adopted, as a guiding example, a value of 1 km s^{-1} when performing 1D calculations.

4.2. Three-dimensional versus one-dimensional bolometric differences in correction

The figures in the Appendix display the bolometric corrections between 3D simulations and the corresponding 1D hydrostatic models with microturbulence = 1 km s^{-1}. The values of BC are reported in Table B.1 to Table 8 for all the filters and, to retrieve the absolute colours, Eqs. (3) and (4) should be used. Considering the SDSS, SkyMapper, 2MASS, and HST-WFC3 systems, the overall deviations are limited to small fraction (less than 5%) from BC_r to BC_{Ks}, but they increase to 10% for BC_u and in BC_g (SDSS) and for $BC_g sky$, $BC_v sky$, and $BC_u sky$ (SkyMapper) where the optical and line crowded region of the spectrum is probed with rather narrow filters (Fig. 4, bottom); these differences decline with increasing effective temperature.

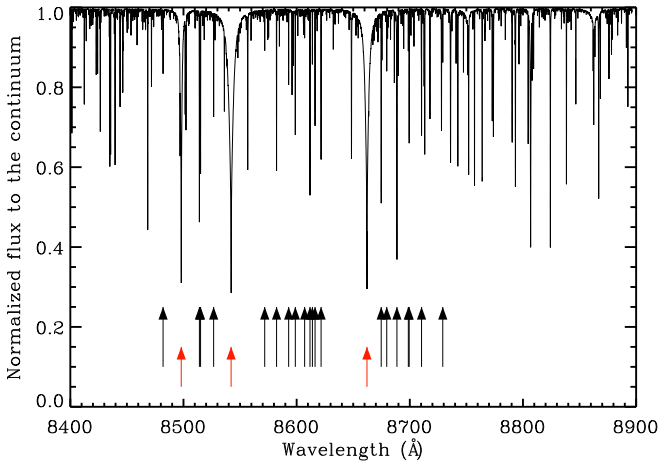

Fig. 5. Flux normalised to the continuum for the solar simulation (Table B.1) in the RVS range (8400–8900 Å). The Fe I lines (black arrows) are from Bigot & Thévenin (2006), while the Ca II triplet are indicated with red arrows.

This behaviour is more or less visible for all the photometric systems; there is no clear correspondence of ΔBC with the other stellar parameters. On a broad scale, the wide infrared photometric systems like 2MASS ($BC_{\rm H}$ and $BC_{\rm Ks}$) and optical *Gaia* ($BC_{\rm G}$) display a noticeable offset with respect to ΔBC = 0.0. This is due to a redistribution of the spectral energy flux among the different filters and is a direct effect of the impact of 3D dynamics and thermodynamic structure on spectral line formation.

Gaia photometric systems return 3D and 1D deviations of less than 3% with higher values for the bluer system (BP). This effect may be not negligible and should become important for future releases of *Gaia* data. For this purpose, part of the spectra presented in this work have already been provided to *Gaia* consortium-CU8[5].

5. Convective velocity shifts for RVS

Measurements of stellar radial velocities are fundamental in order to determine stellar space velocities. This is needed, for example to investigate the kinematic structure of stellar populations in the Galaxy or to monitor for radial velocity variations, either of which would point to the presence of unseen companion(s). Convection plays a crucial role in the formation of spectral lines and deeply influences the shape, shift, and asymmetries of lines in late-type stars (e.g. Asplund et al. 2000a). These stars represent most of the objects that will be observed during the *Gaia* mission. Absorption lines may be blueshifted as a result of convective movements in the stellar atmosphere: bright and rising convective elements contribute more photons than the cool dark shrinking gas, and as a consequence, the absorption lines appear blueshifted (Dravins 1982). However, the convective line shift is not the same for all the spectral lines. Each line has a unique fingerprint in the spectrum that depends on line strength, depth, shift, width, and asymmetry across the granulation pattern depending on their height of formation and sensitivity to the atmospheric conditions. In this context, the line strengths play a major role (Asplund et al. 2000c).

[5] For more details, see the technical note "The 3D spectral library for BP/RP" (Chiavassa et al. 2014c).

Table 2. Central wavelength position, oscillator strength ($\log gf$), and excitation potential (χ) for the 20 Fe I in the spectral domain of RVS (Bigot & Thévenin 2006).

λ [Å]	($\log gf$)	χ [eV]
8481.985	−2.097	4.1860
8514.068	−2.250	2.1980
8515.109	−2.033	3.0180
8526.667	−0.675	4.9130
8571.803	−1.134	5.0100
8582.257	−2.198	2.9900
8592.951	−0.891	4.9560
8598.829	−1.285	4.3860
8607.078	−1.419	5.0100
8611.801	−1.900	2.8450
8613.939	−1.121	4.9880
8616.280	−0.935	4.9130
8621.601	−2.369	2.9490
8674.741	−1.780	2.8310
8679.639	−1.040	4.9660
8688.623	−1.249	2.1760
8698.706	−3.464	2.9900
8699.453	−0.480	4.9550
8710.391	−0.425	4.9130
8729.147	−2.933	3.4150

The aim of the present section is to derive the overall convective shift for 3D simulations. First, we computed the 1D and 3D spectra with a constant resolving power of $\lambda/\Delta\lambda$ = 300 000 from 8470 to 8710 Å for a limited number of 3D simulations (see Table B.1) covering stellar parameters observed by RVS (i.e. [Fe/H] ≥ -2.0). Then, from our spectra we selected only a series of non-blended Fe I lines and masked the others (Fig. 5). The oscillator strengths of these Fe I lines (Table 2) have been accurately determined by Bigot & Thévenin (2006) using 3D RHD simulation where the Fe I and Ca II lines are indicated. It should be noted that the synthetic spectra, when compared to the observations, have to be gravitationally redshifted (e.g. Pasquini et al. 2011) by a certain amount corresponding to the type of star considered (e.g. for the Sun it is 636.486 ± 0.024 m s^{-1} Lindegren & Dravins 2003). Gravitational shifts for late-type dwarfs ($\log g \approx 4.5$) range between 0.7 and 0.8 km s^{-1} and they dramatically decrease with surface gravity down to 0.02–0.03 km s^{-1} for K giant stars with $\log g \approx 1.5$ (Allende Prieto et al. 2013).

The velocity gradient through the photosphere sets the basic shape of the absorption lines in terms of asymmetry and position of the emerging intensity. One way to detect the asymmetries in the line is the bisector[6]. A symmetric profile has a straight vertical bisector (i.e. in the case of hydrostatic 1D spectra). The spectral lines with C-shape bisectors are formed mostly in the upflows (granules) and therefore blueshifted. The reverse C-shapes are generally formed in downflows (Dravins et al. 1981). Reversed C-shape bisectors can be explained by a combination of a steep decline in velocities with height with a flux deficit spanning only a fraction of the red wing of the line profiles (Gray 2010). Different articles show the presence of bisectors revealing asymmetries and wavelength shifts that indicate the presence of granulation for several kinds of stars (e.g. Ramírez et al. 2008; Gray 2009).

[6] Defined as the locus of the midpoints of the spectral line.

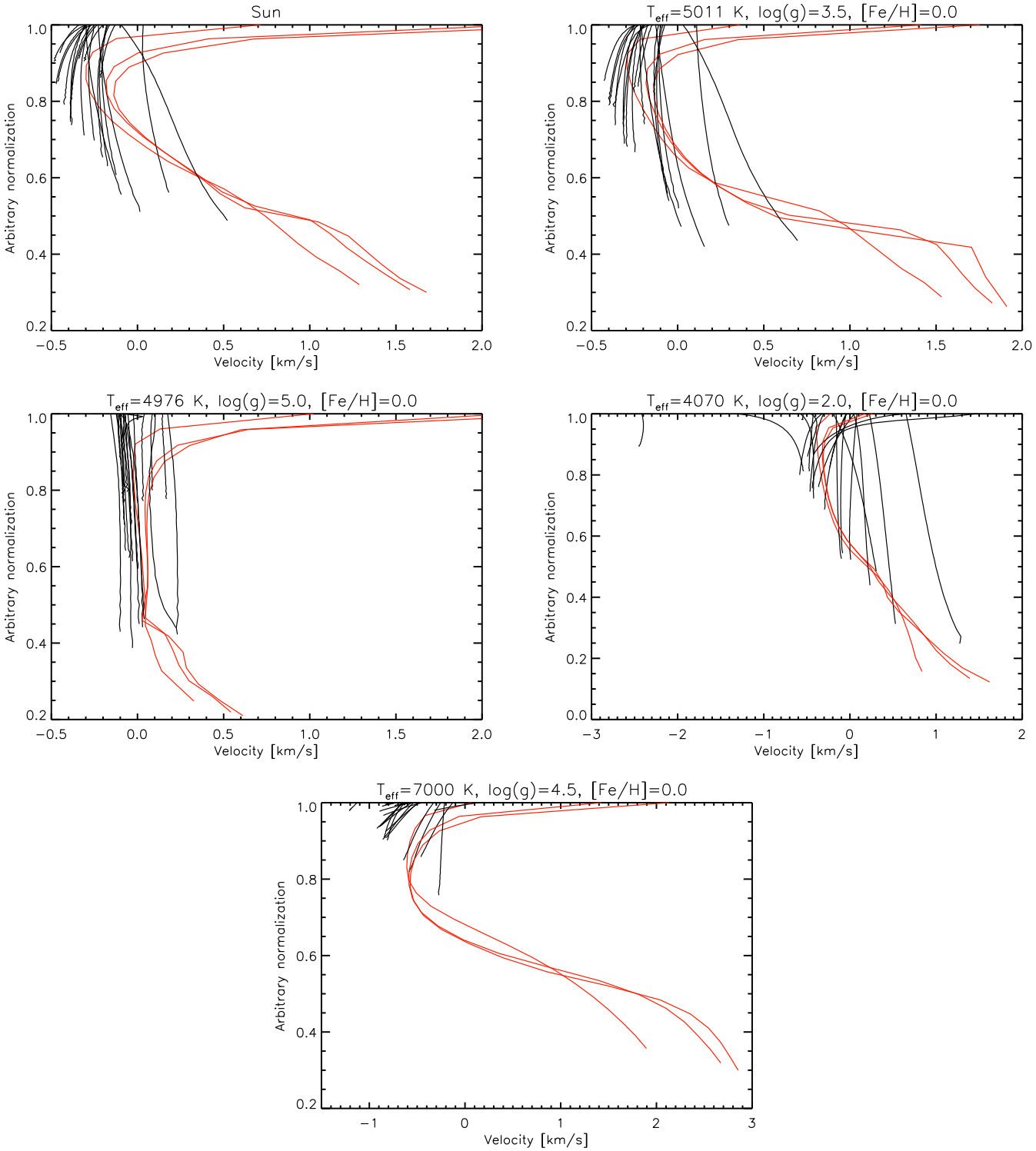

Fig. 6. Line bisectors of the 20 Fe I lines (black) from Bigot & Thévenin (2006) and Ca II triplet (red) for five 3D simulations in the grid.

Figure 6 shows the line bisectors for the Fe I and Ca II triplet lines for stars with different $T_{\rm eff}$ and $\log g$, but with the same metallicity. The gas is strongly horizontally divergent due to mass conservation and its velocities diminish with height. Weak lines (with typically high excitation potential), which form in deeper layers, are more blueshifted than strong lines whose core and part of the wings are formed in higher layers. This effect is particularly visible in Fig. 6 when comparing the solar bisector with the hottest $T_{\rm eff}$ = 7000 K simulations. In addition, the velocity field in 3D simulations of STAGGER-grid largely affects the overall shape of the iron lines in the range of RVS and for all the stars with the strongest effects for Ca II. This has already been shown for other spectral regions (e.g. Asplund et al. 2000b; Allende Prieto et al. 2002; Ramírez et al. 2009; Pereira et al. 2013; Magic et al. 2014).

We determined the convective shift considering only Fe I and only Ca II triplet lines, we cross-correlated each 3D spectrum with the corresponding 1D by using a lag vector corresponding

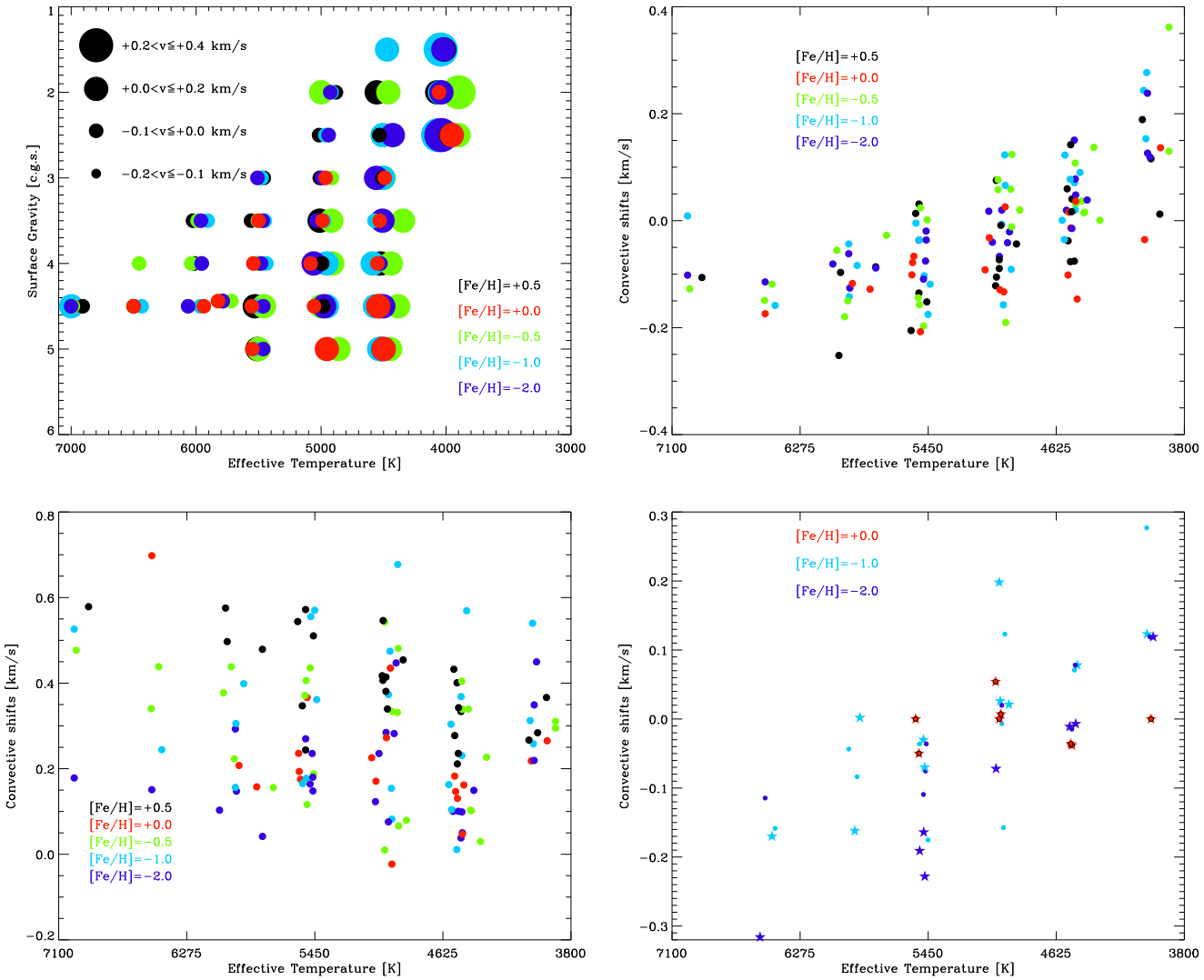

Fig. 7. *Top left panel*: convective shifts predicted by the 3D hydrodynamical simulations for the *Gaia* RVS spectral range and the Fe I lines (see text for details). *Top right panel*: convective shifts from Fe I lines as a function of the effective temperature of the 3D simulations in Table B.1. *Bottom left panel*: convective shifts from Ca II lines. *Bottom right panel*: comparison of convective shifts for a selected number of RHD simulations from this work (stars) with simulations with equivalent stellar parameters from Allende Prieto et al. (2013) (circles). See Table 3 for details.

to radial velocities (RV) in the range $-10 < v < +10\,\mathrm{km\,s^{-1}}$ for Fe I, and $-150 < v < +150\,\mathrm{km\,s^{-1}}$ for Ca II triplet lines, in steps of $0.3\,\mathrm{km\,s^{-1}}$. These velocity ranges were chosen to largely cover the wavelength frequency points of all the single lines. For each RV value, we Doppler-shifted the 1D spectrum and computed its cross-correlation function (CCF) with the 3D spectrum. The final step is to compute the weighted average to obtain the location of the CCF maximum, which corresponds to the actual 3D convective shifts (CS) with respect to 1D models:

$$CS = \frac{\int_{-10}^{+10} RV\,(v) \cdot CCF\,(v)\,\mathrm{d}v}{\int_{-10}^{+10} CCF\,(v)\,\mathrm{d}v} \quad (5)$$

Figure 7 displays the convective shifts for all the simulations either in the HR diagram (top left panel) or as a function of the $T_{\rm eff}$ for the Fe I of Table 2 (top right panel), and for the Ca II triplet lines (bottom left panel). We found that surface gravity and metallicity have a small effect on the convective shifts, as already noticed by Allende Prieto et al. (2013). The values for the Fe I are in the range between −0.235 and +0.361 $\mathrm{km\,s^{-1}}$. The convective shifts of Ca II lines are strongly redshifted (as shown by red bisectors in Fig. 6) and are between −0.023 and +0.698 $\mathrm{km\,s^{-1}}$. In Fig. 7 (top right panel), there is a net correlation of the convective shifts with the effective temperature: $T_{\rm eff} \lessapprox 4500$ K denotes redshifts, while $T_{\rm eff} \gtrapprox 5000$ K denotes blueshifts (except for the hottest $T_{\rm eff} \approx 7000$ K). This result is in agreement with Allende Prieto et al. (2013), who had performed the calculations for a different set of iron lines and found a milder correlation, where $T_{\rm eff}$ with warmer stars tend to exhibit larger blueshifts.

To quantify the differences in the convective shifts, we selected 26 simulations from Table B.1 with the same surface gravity, metallicity, and $\Delta T_{\rm eff} < 50$ K with respect to a subset of CIFIST-grid simulations from Allende Prieto et al. (2013). Convective shifts, as a function of metallicity (Table 3), from RHD simulations in this work are $CS_{\rm Stagger,[Fe/H]=0} = [-0.135, 0.142]$, $CS_{\rm Stagger,[Fe/H]=-1} = [-0.175,\ 0.277]$, and $CS_{\rm Stagger,[Fe/H]=-2} = [-0.114,\ 0.119]\,\mathrm{km\,s^{-1}}$, and from CIFIST-grid simulations $CS_{\rm CIFIST,[Fe/H]=0} = [-0.050,\ 0.054]$, $CS_{\rm CIFIST,[Fe/H]=-1} = [-0.170,\ 0.198]$, and $CS_{\rm CIFIST,[Fe/H]=-2} = [-0.316,\ 0.119]\,\mathrm{km\,s^{-1}}$. The spanned shift values from both grids are similar (Fig. 7,

Table 3. Selected convective shifts for Fe I only ($CS_{\rm Stagger}$ in km s^{-1}) from RHD simulations in this work and from CIFIST-grid simulations ($CS_{\rm CIFIST}$ in km s^{-1}) with equivalent stellar parameters from Allende Prieto et al. (2013).

$T_{\rm eff,Stagger}$	$T_{\rm eff,CIFIST}$	$\log g$	[Fe/H]	$CS_{\rm Stagger}$	$CS_{\rm CIFIST}$	$\Delta_{\rm CS}$
4014	4018	1.50	−0.0	0.116	0.000	0.116
4524	4480	4.00	−0.0	0.040	−0.038	0.078
4532	4509	4.50	−0.0	0.142	−0.036	0.178
5015	4968	2.50	−0.0	−0.122	0.054	−0.176
4992	4954	4.00	−0.0	−0.073	0.000	−0.073
4982	4982	4.50	−0.0	−0.009	0.007	−0.016
5509	5475	4.00	−0.0	−0.135	−0.050	−0.085
5530	5488	4.50	−0.0	0.014	0.000	0.014
4042	4040	1.50	−1.0	0.277	0.123	0.154
4508	4490	2.50	−1.0	0.071	0.078	−0.007
4965	4993	2.50	−1.0	−0.157	0.198	−0.355
4975	4930	3.50	−1.0	−0.007	0.021	−0.028
4956	4986	4.00	−1.0	0.123	0.026	0.097
5450	5481	3.50	−1.0	−0.175	−0.030	−0.145
5506	5473	4.50	−1.0	−0.036	−0.070	0.034
5907	5890	3.50	−1.0	−0.084	0.002	−0.086
5961	5923	4.50	−1.0	−0.043	−0.162	0.119
6435	6456	4.50	−1.0	−0.158	−0.170	0.012
4021	4001	1.50	−2.0	0.119	0.119	−0.000
4524	4500	4.00	−2.0	−0.015	−0.007	−0.008
4502	4539	4.50	−2.0	0.078	−0.011	0.089
4976	5013	4.50	−2.0	0.020	−0.072	0.092
5467	5505	3.50	−2.0	−0.075	−0.191	0.116
5480	5472	4.00	−2.0	−0.109	−0.228	0.119
5462	5479	4.50	−2.0	−0.036	−0.164	0.128
6500	6533	4.50	−2.0	−0.115	−0.316	0.201

Notes. The difference in $T_{\rm eff}$ is set to be smaller than 50 K.

bottom right panel), and show smaller deviations at solar metallicity ($\Delta_{\rm CS} \leqslant 0.195$ km s^{-1}) and slightly larger deviations at [Fe/H] = −1 ($\Delta_{\rm CS} \leqslant 0.370$ km s^{-1}) and [Fe/H] = −2 ($\Delta_{\rm CS} \leqslant 0.221$ km s^{-1}). Apart from the possible numerical differences in the simulations and in the radiative transfer, the shift deviations may also be due to the set of spectral lines considered.

The extraction of accurate radial velocities from RVS needs an appropriate wavelength calibration from convective shifts. This is directly processed in RVS pipeline using the synthetic spectra presented in this work and provided to *Gaia* consortium-CU6[7].

6. Conclusions

We provided synthetic spectra from the STAGGER-grid:

- low-resolution spectra from 1000 to 200 000 Å with a constant resolving power of $\lambda/\Delta\lambda = 20\,000$;
- high-resolution spectra from 8400 to 8900 Å (*Gaia* RVS spectral range), with a constant resolving power of $\lambda/\Delta\lambda = 300\,000$.

We used the low-resolution spectra to compute synthetic colours in the Johnson-Cousins $UBV(RI)_C$, SDSS, 2MASS, *Gaia* systems, SkyMapper, Strömgren, and HST-WFC3. We extracted the bolometric corrections for the 3D simulations and the corresponding 1D hydrostatic models. We probed that 1D versus 3D deviations are limited to small fraction (less than 5%) except for $BC_{\rm u}$ and to a lesser extent $BC_{\rm g}$, where the differences are larger than 10%. Systems *u* and *g* span the optical and line crowded region of the spectrum. Moreover, we showed that there is a clear correlation between effective temperature and 3D and 1D deviations (ΔBC): it decreases with increasing effective temperature.

The *Gaia* photometric system return 3D and 1D deviations of less than 3% with higher values for the bluer filter (BP). This effect should become important for future releases of *Gaia* data. For this purpose, part of the spectra presented in this work have already been provided to *Gaia* consortium-CU8.

We used the high-resolution spectra to denote the impact of the velocity gradient through the photosphere on the basic shape of the absorption lines. For this purpose, we reported the line bisectors of non-blended Fe I and Ca II triplet lines for different stars. We showed that weak lines (high excitation potential), which form in deeper layers, are more blueshifted than strong lines (low excitation potential), whose core and part of the wings are formed in higher layers.

As a final step to derive the overall convective shift for 3D simulations with respect to the reference 1D hydrostatic models, we cross-correlated each 3D spectrum with the corresponding 1D spectrum. The spanned values are between −0.235 and +0.361 km s^{-1}. We showed a net correlation of the convective shifts with the effective temperature: lower $T_{\rm eff}$ denotes redshifts and higher $T_{\rm eff}$ blueshifts; this result is in agreement with Allende Prieto et al. (2013). In addition, we quantified the differences in the convective shifts between a subset of the RHD simulations in this work and the corresponding CIFIST-grid simulations. The spanned shift values from the two grids are similar, and show smaller deviations at solar metallicity. The extraction of accurate radial velocities from RVS spectra need an appropriate wavelength calibration from convection shifts. The spectra presented in this work have been provided to *Gaia* consortium-CU6 to directly process the observed spectra in RVS pipeline.

We have made all the spectra publicly available for the community through the POLLUX database (Palacios et al. 2010). POLLUX[8] is a stellar spectra database proposing access to theoretical data including high-resolution synthetic spectra and spectral energy distributions from several model atmospheres. Continuous development either of the STAGGER-grid simulations or of the spectral synthesis calculations will be uploaded there in the future.

Acknowledgements. L.C. gratefully acknowledges support from the Australian Research Council (grants DP150100250, FT160100402). This work was granted access to the HPC resources of Observatoire de la Côte d'Azur – Mésocentre SIGAMM.

References

Allende Prieto, C., Asplund, M., García López, R. J., & Lambert, D. L. 2002, ApJ, 567, 544
Allende Prieto, C., Koesterke, L., Ludwig, H.-G., Freytag, B., & Caffau, E. 2013, A&A, 550, A103
Asplund, M. 2000, A&A, 359, 755
Asplund, M., Ludwig, H., Nordlund, Å., & Stein, R. F. 2000a, A&A, 359, 669
Asplund, M., Nordlund, Å., Trampedach, R., Allende Prieto, C., & Stein, R. F. 2000b, A&A, 359, 729
Asplund, M., Nordlund, Å., Trampedach, R., & Stein, R. F. 2000c, A&A, 359, 743

[7] For more details, see the technical note "3D spectral library for RVS radial velocities" (Chiavassa et al. 2014b) and the paper on CU6 design and performance (Sartoretti et al., in prep.).

[8] Available at http://pollux.oreme.org

Asplund, M., Grevesse, N., & Sauval, A. J. 2005, in Cosmic Abundances as Records of Stellar Evolution and Nucleosynthesis, eds. T. G. Barnes, III, & F. N. Bash, ASP Conf. Ser., 336, 25
Asplund, M., Grevesse, N., Sauval, A. J., & Scott, P. 2009, ARA&A, 47, 481
Bailer-Jones, C. A. L., Andrae, R., Arcay, B., et al. 2013, A&A, 559, A74
Bessell, M. S. 2000, PASP, 112, 961
Bessell M. S. 2011, PASP, 123, 1442
Bessell, M., & Murphy, S. 2012, PASP, 124, 140
Bessell, M., Bloxham, G., Schmidt, B., et al. 2011, PASP, 123, 789
Bigot, L., & Thévenin, F. 2006, MNRAS, 372, 609
Bigot, L., & Thévenin, F. 2008, in SF2A-2008, 3, eds. C. Charbonnel, F. Combes, & R. Samadi
Bigot, L., Mourard, D., Berio, P., et al. 2011, A&A, 534, L3
Bonifacio, P., Caffau, E., Ludwig, H.-G., et al. 2017, Mem. Soc. Astron. It., 88, 90
Brott, I., & Hauschildt, P. H. 2005, in The Three-Dimensional Universe with Gaia, ed. C. Turon, K. S. O'Flaherty, & M. A. C. Perryman, ESA SP, 576, 565
Caffau, E., Ludwig, H.-G., Steffen, M., Freytag, B., & Bonifacio, P. 2011, Sol. Phys., 268, 255
Cami, J., Sloan, G. C., Markwick-Kemper, A. J., et al. 2009, ApJ, 690, L122
Casagrande, L., & VandenBerg, D. A. 2014, MNRAS, 444, 392
Castelli, F., & Kurucz, R. L. 2004, ArXiv e-prints [arXiv:0405087]
Chiavassa, A., Plez, B., Josselin, E., & Freytag, B. 2009, A&A, 506, 1351
Chiavassa, A., Collet, R., Casagrande, L., & Asplund, M. 2010, A&A, 524, A93
Chiavassa, A., Bigot, L., Thévenin, F., et al. 2011, J. Phys. Conf. Ser., 328, 012012
Chiavassa, A., Bigot, L., Kervella, P., et al. 2012, A&A, 540, A5
Chiavassa, A., Ligi, R., Magic, Z., et al. 2014a, A&A, 567, A115
Chiavassa, A., Thévenin, F., Magic, Z., Collet, R., & Asplund, M. 2014b, 3D spectral library for RVS radial velocities, GAIA-C8-TN-OCA-AC-001-1, Tech. Rep.
Chiavassa, A., Thévenin, F., Magic, Z., Collet, R., & Asplund, M. 2014c, The 3D spectral library for BP/RP, GAIA-C8-TN-OCA-AC-002-1, Tech. Rep.
Chiavassa, A., Pere, C., Faurobert, M., et al. 2015, A&A, 576, A13
Chiavassa, A., Caldas, A., Selsis, F., et al. 2017, A&A, 597, A94
Cohen, M., Wheaton, W. A., & Megeath, S. T. 2003, AJ, 126, 1090
Collet, R., Asplund, M., & Trampedach, R. 2007, A&A, 469, 687
Creevey, O. L., Thévenin, F., Boyajian, T. S., et al. 2012, A&A, 545, A17
Deustua, S., Baggett, S., Brammer, G., et al. 2016, WFC3 Data Handbook. Version 3.0 (Baltimore: STScI) Tech. Rep.
Doi, M., Tanaka, M., Fukugita, M., et al. 2010, AJ, 139, 1628
Dravins, D. 1982, ARA&A, 20, 61
Dravins, D., Lindegren, L., & Nordlund, A. 1981, A&A, 96, 345
Gaia Collaboration (Prusti, T., et al.) 2016, A&A, 595, A1
Gray, D. F. 2009, ApJ, 697, 1032
Gray, D. F. 2010, ApJ, 721, 670
Gray, R. O., Graham, P. W., & Hoyt, S. R. 2001, AJ, 121, 2159
Gunn, J. E., Siegmund, W. A., Mannery, E. J., et al. 2006, AJ, 131, 2332
Gustafsson, B., Edvardsson, B., Eriksson, K., et al. 2008, A&A, 486, 951
Hayek, W., Asplund, M., Carlsson, M., et al. 2010, A&A, 517, A49
Hayek, W., Sing, D., Pont, F., & Asplund, M. 2012, A&A, 539, A102
Jordi, C., Gebran, M., Carrasco, J. M., et al. 2010, A&A, 523, A48
Jørgensen, U. G. 1997, IAU Symp., 178, 441
Katz, D., Munari, U., Cropper, M., et al. 2004, MNRAS, 354, 1223
Kurucz, R. L. 2005, Mem. Soc. Astron. It. Suppl., 8, 189
Lindegren, L., & Dravins, D. 2003, A&A, 401, 1185
Ludwig, H., Caffau, E., Steffen, M., et al. 2009, Mem. Soc. Astron. It., 80, 711
Magic, Z., Collet, R., Asplund, M., et al. 2013, A&A, 557, A26
Magic, Z., Collet, R., & Asplund, M. 2014, A&A, submitted [arXiv:1403.6245]
Magic, Z., Chiavassa, A., Collet, R., & Asplund, M. 2015, A&A, 573, A90
Megessier, C. 1995, A&A, 296, 771
Mihalas, D., Dappen, W., & Hummer, D. G. 1988, ApJ, 331, 815
Nordlund, A. 1982, A&A, 107, 1
Nordlund, Å., Stein, R. F., & Asplund, M. 2009, Liv. Rev. Sol. Phys., 6, 2
Palacios, A., Gebran, M., Josselin, E., et al. 2010, A&A, 516, A13
Pasquini, L., Melo, C., Chavero, C., et al. 2011, A&A, 526, A127
Pereira, T. M. D., Asplund, M., Collet, R., et al. 2013, A&A, 554, A118
Ramírez, I., Allende Prieto, C., & Lambert, D. L. 2008, A&A, 492, 841
Ramírez, I., Allende Prieto, C., Koesterke, L., Lambert, D. L., & Asplund, M. 2009, A&A, 501, 1087
Skartlien R. 2000, ApJ, 536, 465
Stempels, H. C., Piskunov, N., & Barklem, P. S. 2001, in 11th Cambridge Workshop on Cool Stars, Stellar Systems and the Sun, eds. R. J. Garcia Lopez, R. Rebolo, & M. R. Zapaterio Osorio, ASP Conf. Ser., 223, 878
Trampedach, R., Asplund, M., Collet, R., Nordlund, Å., & Stein, R. F. 2013, ApJ, 769, 18

Appendix A: One-dimensional versus three-dimensional bolometric corrections

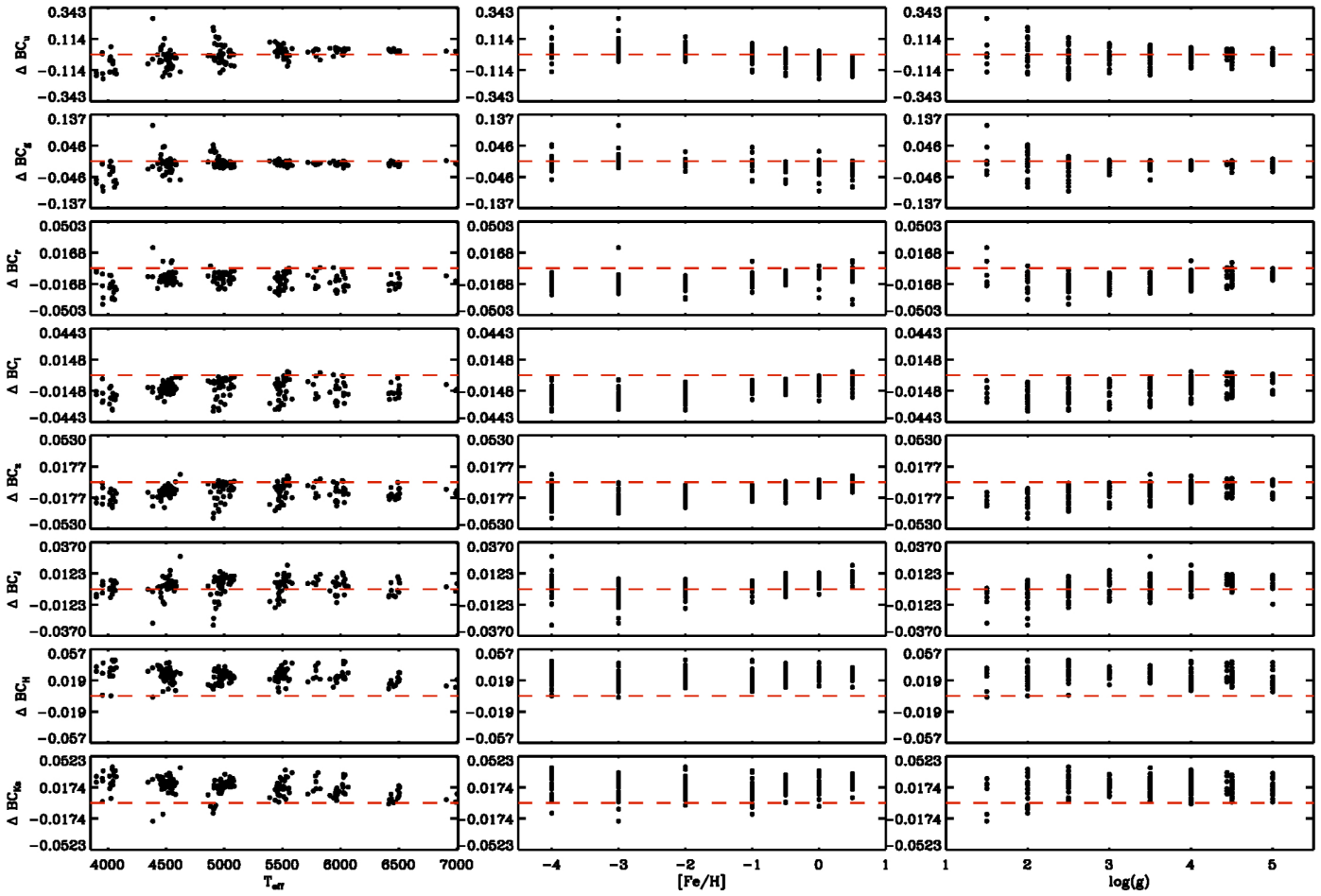

Fig. A.1. Bolometric correction (BC) differences computed for the photometric filters Johnson-Cousins and 2MASS with 3D simulations (Table B.1) and the corresponding 1D hydrostatic models with microturbulence = 1 km s^{-1}: $\Delta BC = BC_{1D} - BC_{3D}$. The red dashed line indicates $\Delta BC = 0.0$.

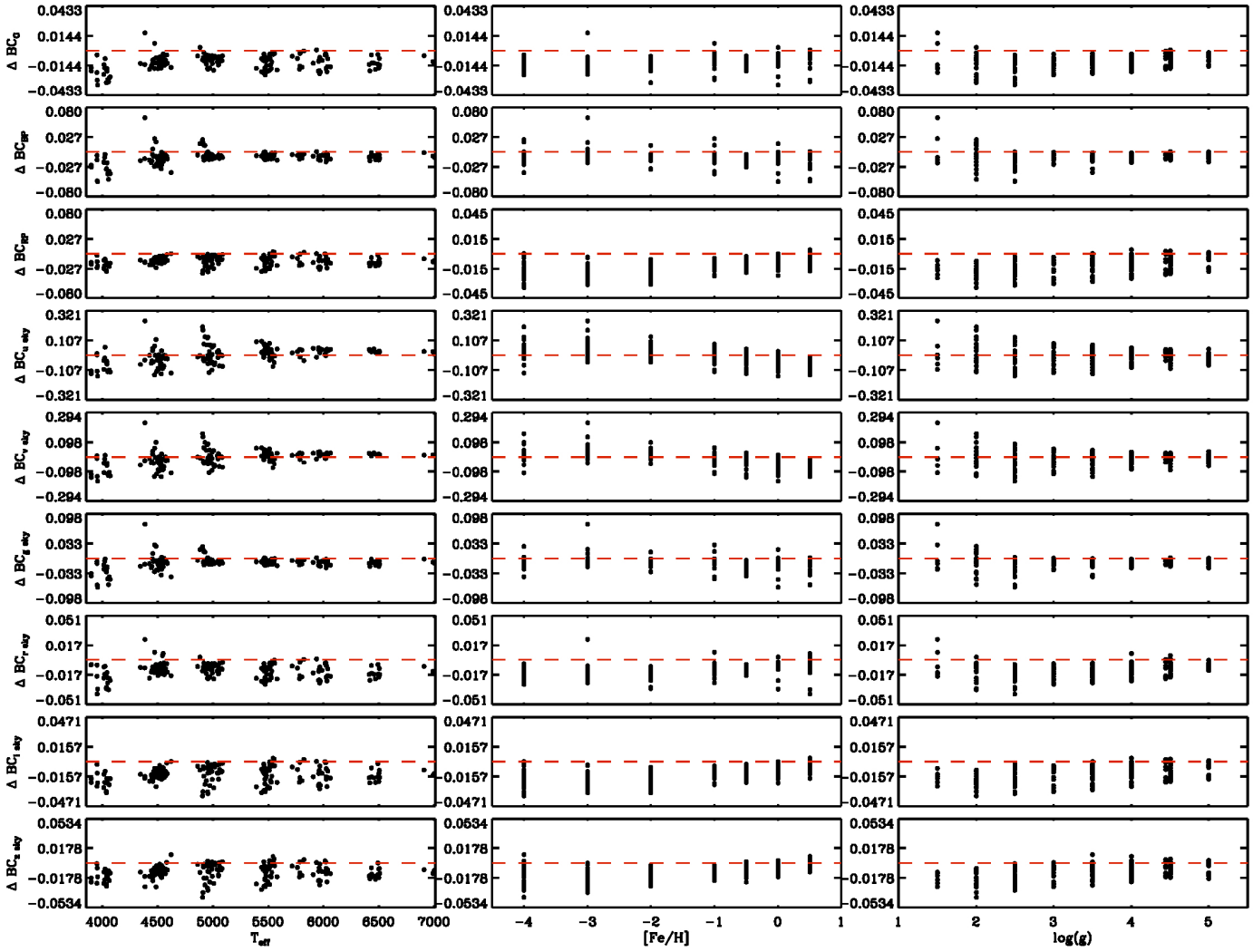

Fig. A.2. Bolometric correction differences for the SkyMapper and *Gaia* photometric filters (Table 1). The notation is the same as in Fig. A.1.

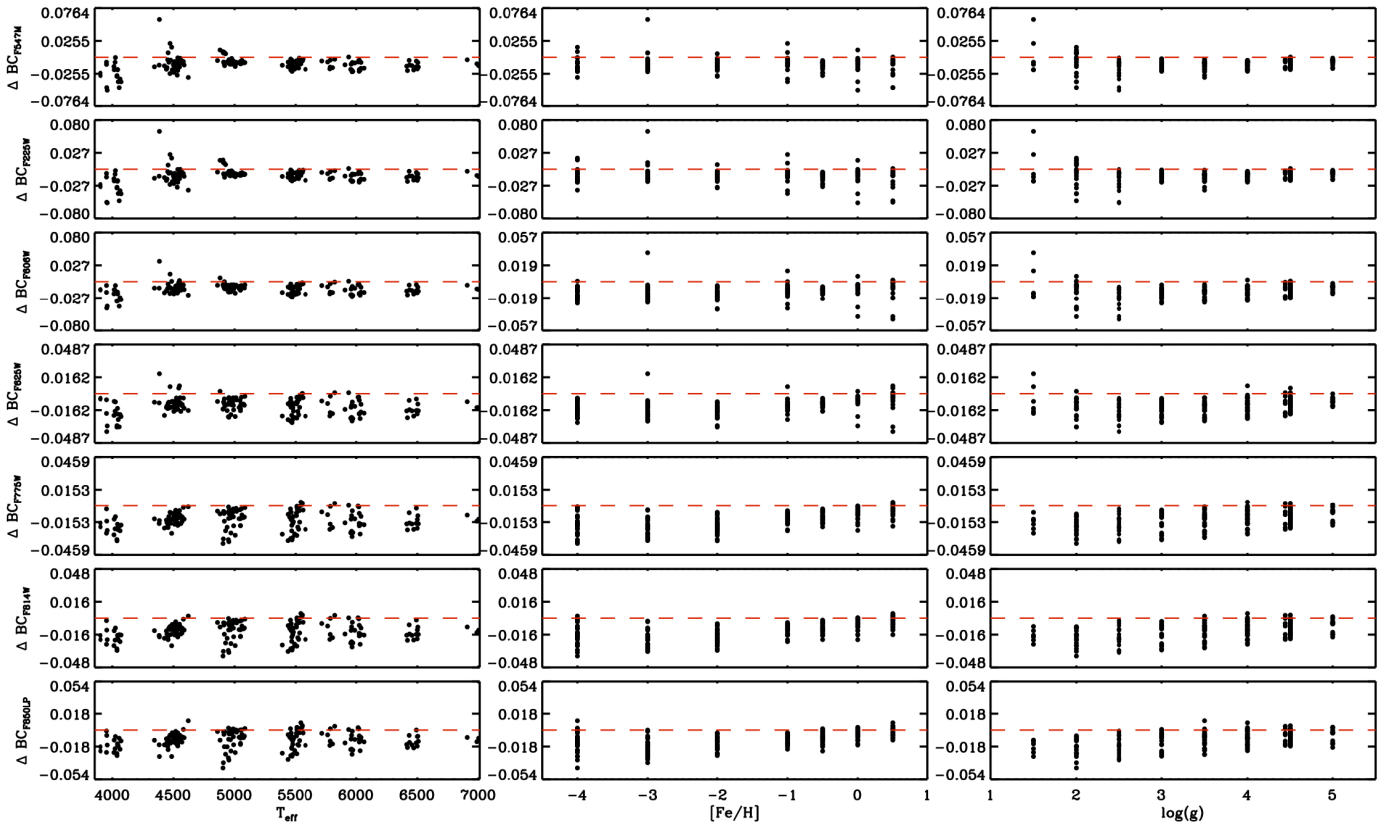

Fig. A.3. Bolometric correction differences for the HST-WFC3 provided in the VEGA system (for the ST and AB systems the differences are similar); first set of filters (Table 1). The notation is the same as in Fig. A.1.

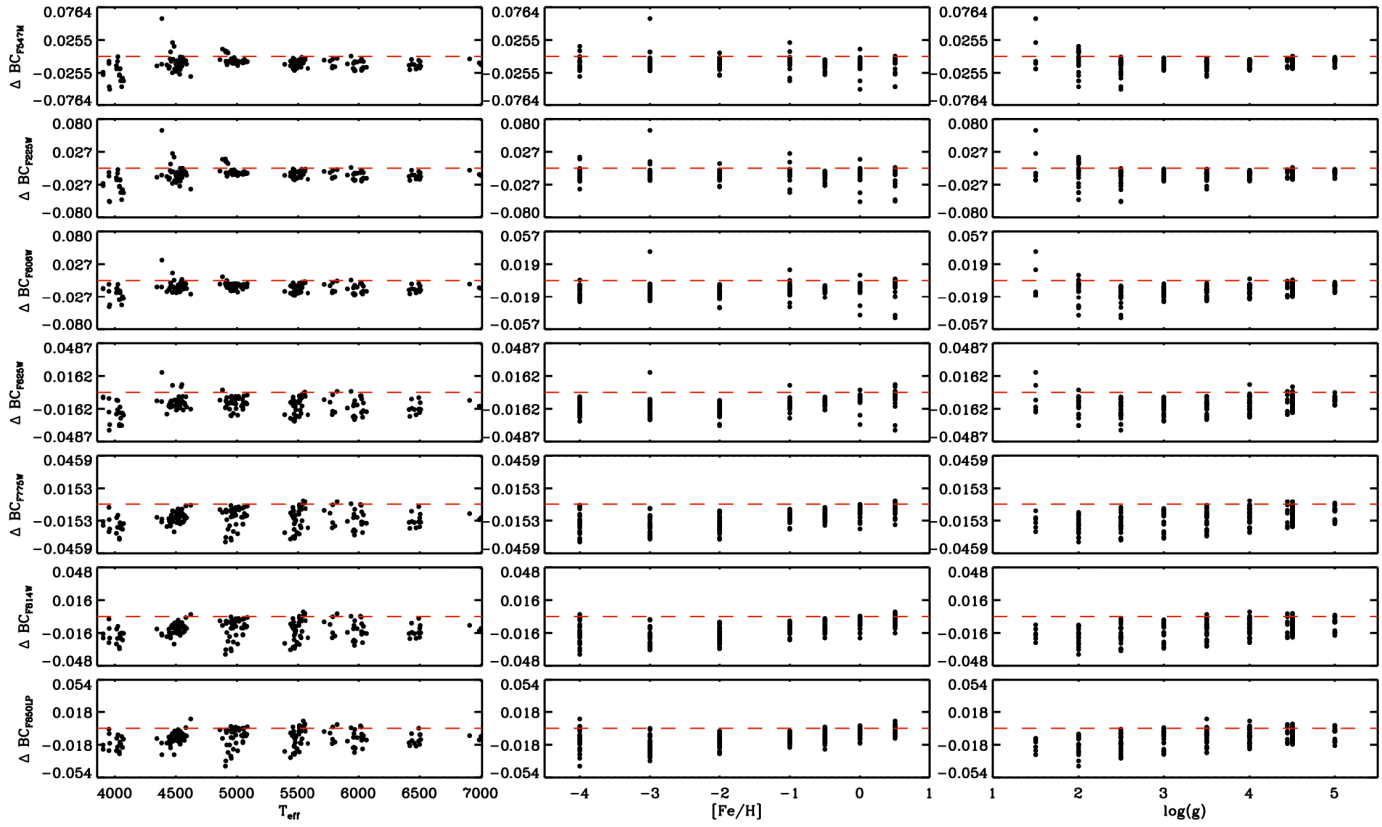

Fig. A.4. Bolometric correction differences for the HST-WFC3 provided in the VEGA system (for ST and AB systems the differences are similar); second set of filters (Table 1). The notation is the same as in Fig. A.1.

Appendix B

Table B.1. RHD simulations' stellar parameters (first three cols.), bolometric Magnitude (M_{bol}), and bolometric correction (BC) for Johnson-Cousins, 2MASS, SDSS, and *Gaia* systems (Table 1).

T_{eff}	log g	[Fe/H]	M_{bol}	BC_U	BC_B	BC_V	BC_R	BC_I	BC_J	BC_H	BC_{Ks}	BC_u	BC_g	BC_r	BC_i	BC_z	BC_G	BC_{BP}	BC_{RP}
4014.99	1.50	0.0	6.320	−3.75310	−2.26910	−0.90560	−0.14050	0.53170	1.58810	2.32330	2.53140	−4.67960	−1.63880	−0.43510	0.02130	0.31350	−0.42180	−1.17700	0.44010
4042.38	1.50	−1.0	6.291	−3.11690	−2.12650	−0.86970	−0.13680	0.52720	1.55730	2.32870	2.50310	−4.01150	−1.54990	−0.42970	0.02220	0.30510	−0.40820	−1.13330	0.43660
4021.90	1.50	−2.0	6.313	−3.24590	−2.23800	−0.90050	−0.14700	0.53780	1.56940	2.32730	2.50270	−4.17080	−1.62720	−0.44840	0.02840	0.32220	−0.42050	−1.17860	0.44480
3951.92	1.50	−3.0	6.389	−3.90090	−2.60760	−1.04190	−0.19200	0.56190	1.61550	2.33340	2.52470	−4.86820	−1.90680	−0.52040	0.03670	0.36450	−0.46890	−1.33700	0.46060
4070.69	2.00	0.0	6.260	−3.47470	−2.14830	−0.85400	−0.10740	0.54590	1.57170	2.29980	2.49240	−4.39490	−1.55290	−0.39570	0.04140	0.31920	−0.38850	−1.11670	0.45590
4056.19	2.00	0.5	6.276	−3.85400	−2.25760	−0.92060	−0.14870	0.56010	1.60690	2.29380	2.50930	−4.79910	−1.63670	−0.45150	0.03890	0.34310	−0.41620	−1.18640	0.45950
3899.43	2.00	−0.5	6.447	−3.49590	−2.36970	−1.05820	−0.25620	0.49620	1.59210	2.40180	2.59540	−4.40270	−1.78920	−0.57300	−0.03710	0.29980	−0.51130	−1.31650	0.39120
4047.76	2.00	−1.0	6.285	−2.91330	−2.07200	−0.87100	−0.14040	0.52420	1.55180	2.32650	2.49650	−3.79910	−1.52820	−0.43160	0.01740	0.30250	−0.40790	−1.12290	0.43260
4037.03	2.00	−2.0	6.296	−2.95540	−2.11670	−0.86700	−0.13370	0.53570	1.55820	2.31110	2.48410	−3.86190	−1.54730	−0.42860	0.02910	0.31640	−0.40330	−1.13120	0.44430
4013.24	2.00	−3.0	6.322	−3.35520	−2.30150	−0.90580	−0.12690	0.58160	1.58900	2.27120	2.46040	−4.30180	−1.66740	−0.43730	0.06690	0.36920	−0.40050	−1.19080	0.48470
4025.21	2.00	−4.0	6.309	−3.55980	−2.40540	−0.92680	−0.10890	0.63070	1.60940	2.21870	2.41580	−4.52770	−1.73930	−0.43200	0.10980	0.42170	−0.38300	−1.21920	0.52890
3958.11	2.50	0.0	6.382	−3.56660	−2.32010	−1.02810	−0.23570	0.51510	1.59780	2.37820	2.57360	−4.48420	−1.74370	−0.54840	−0.01940	0.31200	−0.48920	−1.28330	0.40730
3953.50	2.50	0.5	6.387	−3.80950	−2.40470	−1.11480	−0.30470	0.52780	1.63440	2.37350	2.58690	−4.74740	−1.81650	−0.64260	−0.02810	0.33840	−0.52750	−1.37160	0.40560
3899.65	2.50	−0.5	6.447	−3.38240	−2.35470	−1.08720	−0.28100	0.50300	1.60010	2.40430	2.59230	−4.28350	−1.80050	−0.60420	−0.04080	0.31030	−0.52270	−1.33810	0.39050
4063.17	2.50	−1.0	6.268	−2.78900	−2.03250	−0.86810	−0.13650	0.53330	1.55190	2.31450	2.48120	−3.66800	−1.51230	−0.42730	0.02380	0.31040	−0.40060	−1.11150	0.43930
4037.59	2.50	−2.0	6.296	−2.77250	−2.05380	−0.85520	−0.12540	0.53900	1.55450	2.29540	2.46930	−3.66430	−1.51240	−0.41780	0.03300	0.31850	−0.39290	−1.10840	0.44790
4042.85	2.50	−3.0	6.290	−2.93700	−2.11110	−0.83090	−0.09010	0.59520	1.57280	2.21440	2.40930	−3.85780	−1.52630	−0.39140	0.08580	0.37500	−0.35830	−1.10360	0.50040
3951.87	2.50	−4.0	6.389	−3.26910	−2.30040	−0.89860	−0.09830	0.63760	1.61510	2.16480	2.38120	−4.21420	−1.66940	−0.41890	0.11610	0.43080	−0.36630	−1.18290	0.53650
4472.00	1.50	−1.0	5.852	−2.21550	−1.56460	−0.51380	0.07860	0.62940	1.46770	2.05830	2.20120	−3.09040	−1.04910	−0.17990	0.15820	0.35350	−0.18650	−0.76800	0.55020
4384.64	1.50	−3.0	5.938	−2.61300	−1.81900	−0.61560	0.05090	0.66850	1.51840	2.07870	2.23480	−3.54550	−1.25530	−0.22970	0.18080	0.41100	−0.22330	−0.89270	0.57920
4554.69	2.00	0.0	5.772	−2.44380	−1.54790	−0.46730	0.13820	0.65260	1.46810	2.00720	2.16230	−3.33110	−1.01620	−0.11140	0.18970	0.36460	−0.14540	−0.71970	0.57920
4461.67	2.00	−0.5	5.862	−2.29270	−1.57500	−0.52280	0.08150	0.62970	1.47180	2.06290	2.20930	−3.16770	−1.06080	−0.17630	0.15810	0.35420	−0.18760	−0.77230	0.55100
4498.97	2.00	−1.0	5.826	−2.02690	−1.49220	−0.50110	0.07720	0.61920	1.45210	2.04650	2.18410	−2.89380	−1.00370	−0.17790	0.14940	0.34140	−0.18180	−0.74320	0.54090
4452.94	2.00	−2.0	5.871	−2.06200	−1.55860	−0.53160	0.06150	0.62690	1.46640	2.05450	2.19950	−2.94780	−1.06070	−0.20060	0.15090	0.35670	−0.19770	−0.78270	0.54490
4455.77	2.00	−3.0	5.868	−2.19880	−1.62250	−0.54530	0.07300	0.65900	1.48290	2.03060	2.18220	−3.10880	−1.11000	−0.19620	0.17840	0.39140	−0.19120	−0.80530	0.57330
4485.37	2.00	−4.0	5.839	−2.18230	−1.61150	−0.53590	0.08540	0.67470	1.48090	2.00600	2.15740	−3.10140	−1.10450	−0.18510	0.19360	0.40570	−0.17930	−0.79680	0.58790
4533.90	2.50	0.0	5.792	−2.42220	−1.54340	−0.48380	0.12230	0.64140	1.46840	2.02900	2.17920	−3.31120	−1.02400	−0.12760	0.17660	0.35660	−0.15770	−0.73070	0.56730
4470.97	2.50	0.5	5.853	−2.96950	−1.69780	−0.54020	0.11300	0.65080	1.50870	2.05830	2.22920	−3.89340	−1.13610	−0.14310	0.18090	0.37280	−0.17980	−0.79450	0.57530
4503.34	2.50	−0.5	5.822	−2.14420	−1.51100	−0.50420	0.08910	0.62890	1.45710	2.04320	2.18270	−3.01490	−1.01820	−0.16560	0.15940	0.34990	−0.17610	−0.74480	0.55090
4508.09	2.50	−1.0	5.817	−1.92660	−1.46250	−0.50400	0.07270	0.61160	1.44500	2.04480	2.17960	−2.78780	−0.99160	−0.18090	0.14210	0.33360	−0.18380	−0.73710	0.53370
4426.04	2.50	−2.0	5.897	−1.96700	−1.54550	−0.54940	0.04450	0.60950	1.46430	2.06960	2.21620	−2.84060	−1.06370	−0.21680	0.13270	0.34180	−0.21180	−0.79080	0.52790
4477.40	2.50	−3.0	5.847	−1.95290	−1.53210	−0.52230	0.07420	0.64670	1.46370	2.00770	2.16010	−2.84360	−1.04790	−0.19010	0.16890	0.37590	−0.18320	−0.77040	0.56270
4535.29	2.50	−4.0	5.791	−1.84490	−1.47630	−0.49410	0.09330	0.66230	1.45020	1.96320	2.11390	−2.74040	−1.00810	−0.16990	0.18550	0.38710	−0.16180	−0.73980	0.57780
4508.67	3.00	0.0	5.817	−2.43240	−1.55940	−0.50960	0.10690	0.63360	1.47190	2.05230	2.19880	−3.32140	−1.05050	−0.14450	0.16670	0.35230	−0.17220	−0.75060	0.55840
4490.40	3.00	0.5	5.834	−2.82400	−1.65450	−0.53470	0.11420	0.64960	1.49830	2.05480	2.21750	−3.74320	−1.11560	−0.14020	0.18030	0.37020	−0.17570	−0.78140	0.57380
4503.05	3.00	−1.0	5.822	−1.89600	−1.46140	−0.51820	0.06670	0.60620	1.44450	2.05290	2.18560	−2.75320	−1.00280	−0.18660	0.13630	0.32910	−0.19030	−0.74390	0.52820
4559.76	3.00	−2.0	5.768	−1.66470	−1.38800	−0.47670	0.08100	0.61510	1.42270	1.98970	2.12750	−2.52520	−0.93990	−0.17070	0.14680	0.33350	−0.16840	−0.70350	0.53670
4555.30	3.00	−3.0	5.772	−1.67820	−1.41150	−0.47620	0.09230	0.64410	1.43190	1.94970	2.10060	−2.55210	−0.95830	−0.16520	0.17160	0.36490	−0.15810	−0.71090	0.56230
4534.50	3.00	−4.0	5.792	−1.69370	−1.43200	−0.48720	0.09140	0.65760	1.43870	1.93500	2.09420	−2.57560	−0.98030	−0.17060	0.18120	0.38190	−0.15880	−0.72490	0.57340
4548.87	3.50	0.0	5.778	−2.35730	−1.52710	−0.49890	0.11790	0.64060	1.46320	2.03430	2.17580	−3.24060	−1.03220	−0.13180	0.17550	0.35520	−0.16090	−0.73350	0.56530
4531.27	3.50	0.5	5.795	−2.71390	−1.61440	−0.52540	0.12180	0.65650	1.48990	2.04020	2.19570	−3.62570	−1.09490	−0.13100	0.18760	0.37340	−0.16580	−0.76460	0.57940
4344.11	3.50	−0.5	5.978	−2.42410	−1.70320	−0.64420	0.02020	0.60920	1.50070	2.14480	2.29230	−3.29750	−1.21390	−0.24690	0.12480	0.34900	−0.25070	−0.87740	0.52410
4573.06	3.50	−1.0	5.755	−1.78470	−1.39920	−0.48670	0.08940	0.61390	1.42690	2.01210	2.14120	−2.63660	−0.95540	−0.15930	0.14840	0.32930	−0.16750	−0.70500	0.53750
4508.84	3.50	−2.0	5.816	−1.72960	−1.43710	−0.50780	0.07100	0.61480	1.43680	2.00740	2.15330	−2.58590	−0.98660	−0.18370	0.14390	0.33770	−0.18240	−0.73290	0.53540
4571.34	3.50	−3.0	5.757	−1.59330	−1.38170	−0.46480	0.10020	0.64940	1.42240	1.91350	2.07260	−2.45980	−0.93710	−0.15650	0.17770	0.36800	−0.14850	−0.69500	0.56760
4620.85	3.50	−4.0	5.710	−1.46630	−1.32610	−0.44540	0.10780	0.65470	1.40480	1.87300	2.03130	−2.33620	−0.90080	−0.14800	0.18350	0.37040	−0.13610	−0.67120	0.57240
4524.22	4.00	0.0	5.802	−2.43030	−1.57480	−0.53140	0.10760	0.64220	1.47270	2.05380	2.19560	−3.31140	−1.08310	−0.14460	0.17420	0.35930	−0.17440	−0.76270	0.56480
4549.22	4.00	0.5	5.778	−2.65660	−1.61150	−0.53480	0.11940	0.66340	1.48930	2.03670	2.18880	−3.56000	−1.10480	−0.13440	0.19200	0.37930	−0.16630	−0.76890	0.58340
4441.77	4.00	−0.5	5.881	−2.28050	−1.60600	−0.58340	0.06360	0.62690	1.47940	2.08810	2.22950	−3.14810	−1.13150	−0.19600	0.15070	0.35490	−0.20920	−0.81060	0.54490
4587.16	4.00	−1.0	5.742	−1.79580	−1.40010	−0.48760	0.09840	0.62010	1.42670	2.00310	2.13310	−2.64530	−0.96180	−0.14950	0.15580	0.33330	−0.16230	−0.70200	0.54390
4524.97	4.00	−2.0	5.801	−1.72580	−1.42910	−0.50050	0.08470	0.62750	1.43500	1.98070	2.13130	−2.57980	−0.98180	−0.16980	0.15730	0.34810	−0.17090	−0.72310	0.54790
4517.64	4.00	−3.0	5.808	−1.66100	−1.42450	−0.48450	0.09720	0.65910	1.43670	1.90820	2.08050	−2.52650	−0.97230	−0.16350	0.18420	0.38210	−0.15380	−0.71680	0.57570
4580.60	4.00	−4.0	5.748	−1.49510	−1.35310	−0.45580	0.10980	0.66660	1.41430	1.85260	2.02610	−2.36350	−0.92270	−0.14940	0.19310	0.38520	−0.13590	−0.68330	0.58300
4532.22	4.50	0.0	5.794	−2.46210	−1.59380	−0.54300	0.11020	0.65210	1.47610	2.04950	2.19140	−3.33990	−1.10600	−0.14280	0.18240	0.36800	−0.17400	−0.77120	0.57240
4543.15	4.50	0.5	5.783	−2.65550	−1.64110	−0.55840	0.11090	0.67100	1.49540	2.04080	2.19370	−3.55180	−1.14040	−0.14560	0.19540	0.38810	−0.17420	−0.78970	0.58690
4383.32	4.50	−0.5	5.939	−2.44210	−1.70270	−0.63540	0.04670	0.63370	1.49980	2.11150	2.25940	−3.31230	−1.22150	−0.21880	0.15100	0.36780	−0.23090	−0.86400	0.54770
4569.29	4.50	−1.0	5.759	−1.88740	−1.44200	−0.50720	0.10140	0.63080	1.43760	2.00870	2.14160	−2.73700	−1.00230	−0.14850	0.16470	0.34510	−0.16530	−0.72080	0.55310
4502.45	4.50	−2.0	5.823	−1.80750	−1.46400	−0.51140	0.09260	0.64530	1.44530	1.96500	2.12500	−2.66330	−1.01120	−0.16520	0.17310	0.36750	−0.16720	−0.73560	0.56420
4526.03	5.00	0.0	5.800	−2.53060	−1.63450	−0.56170	0.11040	0.66540	1.48360	2.04650	2.19060	−3.40670	−1.14470	−0.14510	0.19250	0.38170	−0.17640	−0.78950	0.58260

Table B.1. continued.

$T_{\rm eff}$	$\log g$	[Fe/H]	$M_{\rm bol}$	$BC_{\rm U}$	$BC_{\rm B}$	$BC_{\rm V}$	$BC_{\rm R}$	$BC_{\rm I}$	$BC_{\rm J}$	$BC_{\rm H}$	$BC_{\rm Ks}$	$BC_{\rm u}$	$BC_{\rm g}$	$BC_{\rm r}$	$BC_{\rm i}$	$BC_{\rm z}$	$BC_{\rm G}$	$BC_{\rm BP}$	$BC_{\rm RP}$
4447.10	5.00	−0.5	5.876	−2.38690	−1.65720	−0.59700	0.08140	0.65580	1.48830	2.06250	2.21000	−3.25500	−1.17990	−0.18080	0.17770	0.38180	−0.19960	−0.82390	0.57090
4535.47	5.00	−1.0	5.791	−2.02130	−1.50860	−0.53300	0.10480	0.65280	1.45520	2.00600	2.14670	−2.87420	−1.06100	−0.14990	0.18190	0.36990	−0.16790	−0.74980	0.57140
4881.31	2.00	0.0	5.472	−1.85600	−1.25750	−0.31260	0.22580	0.68500	1.37760	1.81390	1.95050	−2.72730	−0.78050	−0.00840	0.23980	0.36540	−0.04640	−0.54830	0.61700
4915.99	2.00	−1.0	5.441	−1.44220	−1.13310	−0.30090	0.18660	0.65110	1.33750	1.79320	1.91320	−2.30660	−0.70420	−0.04620	0.20420	0.33450	−0.05710	−0.52190	0.58110
4926.40	2.00	−2.0	5.432	−1.34090	−1.10990	−0.30720	0.17860	0.65220	1.33030	1.77580	1.89650	−2.22010	−0.70160	−0.05610	0.20220	0.33790	−0.06010	−0.52350	0.57980
4907.94	2.00	−3.0	5.448	−1.33290	−1.11580	−0.31880	0.17220	0.65590	1.33580	1.77730	1.90090	−2.22150	−0.71570	−0.06510	0.20260	0.34500	−0.06540	−0.53470	0.58150
4905.26	2.00	−4.0	5.450	−1.31800	−1.11680	−0.32140	0.17000	0.65720	1.33590	1.77420	1.89900	−2.20890	−0.71960	−0.06810	0.20270	0.34730	−0.06690	−0.53770	0.58210
5015.94	2.50	0.0	5.353	−1.62160	−1.12750	−0.26400	0.24070	0.67640	1.33360	1.75120	1.87470	−2.48800	−0.68310	0.01380	0.23750	0.34640	−0.02060	−0.48580	0.61100
4950.97	2.50	−0.5	5.410	−1.46410	−1.12260	−0.28930	0.20120	0.65640	1.33150	1.77560	1.89620	−2.32290	−0.69250	−0.02930	0.21170	0.33560	−0.04630	−0.50820	0.58770
4965.89	2.50	−1.0	5.397	−1.30120	−1.07870	−0.29020	0.18260	0.63700	1.31510	1.77130	1.88540	−2.15760	−0.66800	−0.04680	0.19220	0.31700	−0.05470	−0.50120	0.56810
4939.03	2.50	−2.0	5.421	−1.22650	−1.08470	−0.30980	0.16770	0.63670	1.31660	1.76870	1.88800	−2.09240	−0.68770	−0.06530	0.18740	0.32160	−0.06650	−0.51850	0.56490
4948.74	2.50	−3.0	5.412	−1.18400	−1.07210	−0.31190	0.16680	0.64250	1.31290	1.74910	1.87140	−2.05810	−0.68720	−0.06770	0.19100	0.32840	−0.06530	−0.51850	0.56890
4953.38	2.50	−4.0	5.408	−1.15390	−1.06350	−0.31300	0.16320	0.64060	1.30950	1.74280	1.86550	−2.03030	−0.68490	−0.07170	0.18830	0.32720	−0.06690	−0.51840	0.56660
5010.39	3.00	0.0	5.358	−1.60350	−1.12280	−0.26930	0.23460	0.67050	1.33290	1.75990	1.88080	−2.46850	−0.68320	0.00800	0.23110	0.34180	−0.02510	−0.48820	0.60510
4963.15	3.00	0.5	5.399	−2.01830	−1.22030	−0.28690	0.25740	0.69550	1.37290	1.78610	1.92160	−2.90900	−0.74410	0.02810	0.25630	0.36760	−0.02140	−0.51540	0.63150
4912.91	3.00	−0.5	5.444	−1.48350	−1.14370	−0.31040	0.18750	0.64870	1.34060	1.80810	1.92460	−2.33910	−0.71470	−0.04420	0.20190	0.33170	−0.06000	−0.52690	0.57930
4990.00	3.00	−1.0	5.376	−1.23520	−1.05870	−0.28900	0.18010	0.63000	1.30440	1.76130	1.87240	−2.08530	−0.65640	−0.04790	0.18620	0.30840	−0.05510	−0.49430	0.56170
4991.62	3.00	−2.0	5.375	−1.10840	−1.04440	−0.29980	0.16590	0.62510	1.29330	1.73740	1.85460	−1.96400	−0.65950	−0.06400	0.17830	0.30590	−0.06390	−0.50080	0.55440
4970.32	3.00	−3.0	5.393	−1.08960	−1.05480	−0.31250	0.16100	0.63320	1.29860	1.72860	1.85230	−1.95230	−0.67740	−0.07250	0.18260	0.31770	−0.06820	−0.51360	0.56000
5005.01	3.00	−4.0	5.363	−1.02090	−1.02550	−0.30670	0.15890	0.62840	1.28370	1.70360	1.82670	−1.88520	−0.66040	−0.07370	0.17810	0.31130	−0.06660	−0.50360	0.55520
5011.53	3.50	0.0	5.357	−1.60830	−1.11830	−0.27140	0.23210	0.66630	1.33220	1.76670	1.88440	−2.47170	−0.68150	0.00630	0.22730	0.33790	−0.02680	−0.48760	0.60130
4988.91	3.50	0.5	5.377	−1.94540	−1.19200	−0.28030	0.25750	0.69200	1.36290	1.77640	1.90760	−2.83360	−0.72660	0.02990	0.25360	0.36300	−0.01820	−0.50420	0.62830
4917.82	3.50	−0.5	5.439	−1.47540	−1.13940	−0.31360	0.18630	0.64600	1.33880	1.81020	1.92450	−2.32810	−0.71460	−0.04500	0.19960	0.32890	−0.06120	−0.52660	0.57690
4975.93	3.50	−1.0	5.388	−1.23620	−1.06800	−0.29970	0.17470	0.62560	1.30730	1.77390	1.88400	−2.08140	−0.66750	−0.05340	0.18150	0.30520	−0.06130	−0.50220	0.55730
5036.62	3.50	−2.0	5.336	−1.03470	−1.01790	−0.29250	0.16610	0.61710	1.27520	1.71280	1.82790	−1.88270	−0.64050	−0.06150	0.17250	0.29440	−0.06140	−0.48780	0.54740
5047.83	3.50	−3.0	5.326	−0.96660	−1.00740	−0.29740	0.16210	0.62210	1.26750	1.68170	1.80270	−1.82030	−0.64280	−0.06790	0.17490	0.30090	−0.06260	−0.49050	0.55030
5047.65	3.50	−4.0	5.326	−0.92830	−1.00340	−0.30440	0.15450	0.61880	1.26280	1.67270	1.79580	−1.78380	−0.64680	−0.07650	0.17000	0.29900	−0.06810	−0.49560	0.54600
4992.30	4.00	0.0	5.374	−1.65750	−1.13970	−0.28430	0.22940	0.66690	1.33920	1.78180	1.89940	−2.51940	−0.70140	0.00290	0.22730	0.34010	−0.03200	−0.49910	0.60170
5083.68	4.00	0.5	5.295	−1.81620	−1.12350	−0.24970	0.27320	0.69200	1.33530	1.73100	1.85530	−2.69810	−0.67430	0.05010	0.25840	0.35530	0.00120	−0.46590	0.63020
4910.47	4.00	−0.5	5.446	−1.50710	−1.15360	−0.32320	0.18670	0.64700	1.34290	1.81920	1.93320	−2.35760	−0.72940	−0.04480	0.20080	0.33020	−0.06370	−0.53380	0.57810
4956.78	4.00	−1.0	5.405	−1.26990	−1.08980	−0.31280	0.17380	0.62680	1.31480	1.78840	1.89940	−2.11150	−0.68840	−0.05490	0.18240	0.30750	−0.06600	−0.51360	0.55850
5059.64	4.00	−2.0	5.316	−1.00690	−1.01250	−0.28900	0.16920	0.61650	1.26760	1.69860	1.81470	−1.84930	−0.63570	−0.05750	0.17320	0.29180	−0.05880	−0.48260	0.54730
5049.09	4.00	−3.0	5.325	−0.95400	−1.01840	−0.29950	0.16420	0.62660	1.26650	1.66930	1.79600	−1.80280	−0.65070	−0.06660	0.17910	0.30530	−0.06210	−0.49370	0.55430
5072.94	4.00	−4.0	5.304	−0.88740	−0.99970	−0.30200	0.15690	0.61980	1.25250	1.64710	1.77460	−1.73790	−0.64440	−0.07400	0.17170	0.29840	−0.06600	−0.49210	0.54710
4982.27	4.50	0.0	5.383	−1.72500	−1.16460	−0.29680	0.23170	0.67060	1.34610	1.79300	1.91140	−2.58520	−0.72470	0.00480	0.23130	0.34400	−0.03450	−0.50950	0.60550
5056.36	4.50	0.5	5.319	−1.88710	−1.15520	−0.26760	0.26980	0.69220	1.34570	1.75190	1.87680	−2.76700	−0.70440	0.04610	0.25810	0.35810	−0.00620	−0.48200	0.63050
4953.63	4.50	−1.0	5.408	−1.30860	−1.10260	−0.31920	0.17860	0.63060	1.31920	1.79400	1.90580	−2.14780	−0.70140	-0.05010	0.18690	0.31060	−0.06550	−0.51780	0.56260
4976.19	4.50	−2.0	5.388	−1.12990	−1.07590	−0.31240	0.17020	0.63070	1.29880	1.73600	1.86150	−1.97110	−0.68450	−0.06050	0.18430	0.31130	−0.06570	−0.51170	0.56000
5079.81	4.50	−3.0	5.299	−0.93440	−1.00930	−0.28990	0.17290	0.63270	1.25750	1.63920	1.77090	−1.78110	−0.64150	−0.05750	0.18640	0.30880	−0.05410	−0.48420	0.56050
4969.79	4.50	−4.0	5.394	−0.99560	−1.06860	−0.32560	0.15760	0.64080	1.28800	1.67600	1.81900	−1.84780	−0.69690	−0.07950	0.18760	0.32670	−0.07210	−0.52490	0.56540
4976.20	5.00	0.0	5.388	−1.80450	−1.18960	−0.30900	0.23590	0.67520	1.35290	1.80360	1.92170	−2.66340	−0.74840	0.00890	0.23660	0.34830	−0.03580	−0.51910	0.61050
4953.82	5.00	0.5	5.408	−2.06940	−1.26350	−0.32520	0.25260	0.69740	1.38040	1.81150	1.94240	−2.94810	−0.80270	0.02370	0.25750	0.37140	−0.03290	−0.54080	0.63250
4860.02	5.00	−0.5	5.491	−1.69170	−1.22730	−0.35980	0.18960	0.65750	1.36700	1.85490	1.97290	−2.54240	−0.79760	−0.04420	0.21030	0.34330	−0.07360	−0.56810	0.58820
4971.82	5.00	−1.0	5.392	−1.34160	−1.10480	−0.31670	0.18980	0.63850	1.31870	1.78420	1.89690	−2.17970	−0.70420	−0.03820	0.19630	0.31600	−0.05840	−0.51340	0.57090
4980.19	5.00	−2.0	5.385	−1.16660	−1.08500	−0.30950	0.18140	0.64380	1.30190	1.72070	1.85140	−2.00770	−0.69000	−0.05020	0.19760	0.32340	−0.05790	−0.51010	0.57260
5043.95	5.00	−3.0	5.329	−0.98540	−1.03600	−0.29540	0.17780	0.64540	1.27090	1.64160	1.78140	−1.83240	−0.66010	−0.05510	0.19740	0.32370	−0.05260	−0.49410	0.57210
4950.01	5.00	−4.0	5.411	−1.02750	−1.08610	−0.32710	0.16400	0.65270	1.29530	1.66540	1.81680	−1.88020	−0.70860	−0.07490	0.19850	0.33960	−0.06840	−0.52960	0.57640
5390.37	2.50	−2.0	5.041	−0.82020	−0.79850	−0.19050	0.20750	0.60490	1.16860	1.52300	1.62440	−1.69170	−0.46740	−0.00540	0.17540	0.25740	−0.00210	−0.36480	0.54180
5436.69	2.50	−3.0	5.004	−0.74360	−0.76850	−0.19050	0.19770	0.59290	1.14600	1.49030	1.59150	−1.61830	−0.45280	−0.01400	0.16340	0.24430	−0.00580	−0.35830	0.52960
5459.13	3.00	0.0	4.986	−1.08180	−0.83640	−0.13880	0.27850	0.65050	1.18980	1.51360	1.61770	−1.94170	−0.45620	0.07000	0.22980	0.28990	0.04550	−0.33170	0.59260
5479.60	3.00	−0.5	4.970	−0.90320	−0.79180	−0.14620	0.24700	0.62080	1.16170	1.49630	1.59370	−1.76010	−0.43380	0.03930	0.19900	0.26220	0.02950	−0.32920	0.56200
5476.23	3.00	−1.0	4.972	−0.81420	−0.78110	−0.16190	0.22670	0.60550	1.14950	1.48940	1.58670	−1.67100	−0.43750	0.01810	0.18220	0.24920	0.01520	−0.33830	0.54560
5509.14	3.00	−2.0	4.946	−0.69810	−0.75540	−0.18090	0.20020	0.58320	1.12170	1.45720	1.55500	−1.55960	−0.43710	−0.00860	0.15760	0.22820	−0.00280	−0.34620	0.52160
5459.30	3.00	−3.0	4.986	−0.67650	−0.77320	−0.20260	0.18300	0.57740	1.12910	1.47530	1.57530	−1.53840	−0.46070	−0.02840	0.14800	0.22770	−0.01860	−0.36700	0.51380
5469.82	3.00	−4.0	4.977	−0.65020	−0.77020	−0.20640	0.17690	0.57180	1.12170	1.46520	1.56580	−1.51210	−0.46190	−0.03460	0.14200	0.22230	−0.02310	−0.36940	0.50800
5560.38	3.50	0.0	4.906	−0.96890	−0.78500	−0.12210	0.27880	0.63790	1.15520	1.46520	1.56360	−1.82320	−0.41820	0.07400	0.22080	0.27090	0.05240	−0.30700	0.58140
5505.98	3.50	−0.5	4.949	−0.86310	−0.78730	−0.14720	0.24470	0.61600	1.15180	1.48590	1.58080	−1.71280	−0.43160	0.03770	0.19500	0.25570	0.02780	−0.32770	0.55740
5450.91	3.50	−1.0	4.992	−0.79730	−0.80110	−0.17530	0.21780	0.60060	1.15430	1.50760	1.60290	−1.64430	−0.45460	0.00820	0.17600	0.24610	0.00530	−0.35150	0.54010
5467.28	3.50	−2.0	4.979	−0.69010	−0.79070	−0.19890	0.19070	0.58080	1.13170	1.48070	1.57850	−1.54010	−0.46540	−0.02010	0.15330	0.22870	−0.01530	−0.36650	0.51820
5474.46	3.50	−3.0	4.974	−0.63520	−0.78550	−0.21190	0.17500	0.57030	1.11900	1.46290	1.56310	−1.48740	−0.47210	−0.03680	0.14080	0.22000	−0.02700	−0.37560	0.50640
5490.94	3.50	−4.0	4.960	−0.60100	−0.78120	−0.21870	0.16520	0.56060	1.10820	1.45220	1.55150	−1.45300	−0.47410	−0.04640	0.13060	0.21050	−0.03450	−0.37960	0.49650

Table B.1. continued.

$T_{\rm eff}$	log g	[Fe/H]	$M_{\rm bol}$	$BC_{\rm U}$	$BC_{\rm B}$	$BC_{\rm V}$	$BC_{\rm R}$	$BC_{\rm I}$	$BC_{\rm J}$	$BC_{\rm H}$	$BC_{\rm Ks}$	$BC_{\rm u}$	$BC_{\rm g}$	$BC_{\rm r}$	$BC_{\rm i}$	$BC_{\rm z}$	$BC_{\rm G}$	$BC_{\rm BP}$	$BC_{\rm RP}$
5509.78	4.00	0.0	4.946	−1.02250	−0.81670	−0.13570	0.27720	0.64210	1.17320	1.49830	1.59590	−1.87210	−0.44260	0.07070	0.22330	0.27800	0.04630	−0.32270	0.58500
5542.42	4.00	0.5	4.920	−1.21110	−0.83140	−0.11970	0.31630	0.67320	1.18930	1.48680	1.59160	−2.07400	−0.44380	0.10990	0.25810	0.30310	0.07120	−0.31040	0.61820
5513.71	4.00	−0.5	4.943	−0.85020	−0.78790	−0.14990	0.24220	0.61180	1.14860	1.48830	1.57990	−1.69360	−0.43210	0.03570	0.19130	0.25090	0.02550	−0.32850	0.55340
5437.76	4.00	−1.0	5.003	−0.79930	−0.81480	−0.18240	0.21510	0.59910	1.15810	1.52100	1.61420	−1.63930	−0.46520	0.00530	0.17420	0.24520	0.00110	−0.35840	0.53850
5480.60	4.00	−2.0	4.969	−0.66620	−0.79900	−0.20260	0.18810	0.57760	1.12580	1.47340	1.57090	−1.50870	−0.47140	−0.02270	0.15040	0.22470	−0.01870	−0.37010	0.51490
5582.06	4.00	−3.0	4.889	−0.55510	−0.76090	−0.20610	0.16940	0.55320	1.07930	1.40670	1.50300	−1.39990	−0.45430	−0.03940	0.12710	0.19680	−0.02900	−0.36420	0.49050
5523.51	4.00	−4.0	4.935	−0.56420	−0.78730	−0.22270	0.16140	0.55580	1.09460	1.43000	1.53000	−1.40920	−0.47970	−0.05020	0.12640	0.20410	−0.03890	−0.38300	0.49150
5530.74	4.50	0.0	4.929	−1.02080	−0.81610	−0.13430	0.28030	0.64200	1.16930	1.49320	1.58920	−1.86610	−0.44100	0.07450	0.22450	0.27660	0.04830	−0.32010	0.58560
5554.75	4.50	0.5	4.910	−1.21550	−0.83210	−0.11950	0.31850	0.67280	1.18760	1.48520	1.58870	−2.07540	−0.44380	0.11290	0.25850	0.30220	0.07240	−0.30890	0.61840
5457.22	4.50	−0.5	4.987	−0.91310	−0.82770	−0.16420	0.24350	0.62030	1.17060	1.52390	1.61650	−1.75180	−0.46190	0.03480	0.19810	0.26280	0.02050	−0.34640	0.56130
5506.04	4.50	−1.0	4.949	−0.75260	−0.79550	−0.17240	0.21990	0.59470	1.13760	1.48950	1.58030	−1.58720	−0.44910	0.01220	0.17280	0.23600	0.00660	−0.34520	0.53540
5462.38	4.50	−2.0	4.983	−0.67600	−0.82030	−0.20600	0.19180	0.58460	1.13500	1.48320	1.58370	−1.51290	−0.48530	−0.02000	0.15690	0.23250	−0.01870	−0.37670	0.52150
5517.41	4.50	−3.0	4.940	−0.58380	−0.80280	−0.21510	0.17620	0.57180	1.10550	1.43390	1.53740	−1.42380	−0.48440	−0.03610	0.14290	0.21930	−0.02900	−0.38030	0.50750
5531.84	4.50	−4.0	4.928	−0.54970	−0.80040	−0.22400	0.16470	0.56120	1.09390	1.42120	1.52480	−1.39030	−0.48890	−0.04770	0.13160	0.20920	−0.03820	−0.38650	0.49650
5509.50	5.00	0.0	4.946	−1.08990	−0.84050	−0.14030	0.28640	0.64890	1.18130	1.51060	1.60770	−1.93310	−0.45760	0.08000	0.23180	0.28430	0.04880	−0.32750	0.59300
5550.69	5.00	0.5	4.913	−1.27800	−0.84870	−0.12150	0.32560	0.67680	1.19420	1.49360	1.59840	−2.13540	−0.45410	0.12060	0.26370	0.30590	0.07460	−0.31120	0.62360
5528.91	5.00	−1.0	4.931	−0.75360	−0.79470	−0.16850	0.22590	0.59690	1.13360	1.48250	1.57240	−1.58430	−0.44640	0.01900	0.17650	0.23610	0.01080	−0.34060	0.53820
5463.42	5.00	−2.0	4.982	−0.68880	−0.82760	−0.20200	0.19950	0.59230	1.13890	1.48120	1.58480	−1.52290	−0.48740	−0.01270	0.16520	0.23950	−0.01350	−0.37490	0.52920
5468.24	5.00	−3.0	4.978	−0.62010	−0.83010	−0.21800	0.18420	0.58830	1.12600	1.45040	1.56140	−1.45890	−0.50250	−0.03070	0.15760	0.23840	−0.02570	−0.38900	0.52280
5474.24	5.00	−4.0	4.974	−0.58920	−0.83070	−0.22720	0.17450	0.58120	1.11790	1.43980	1.55230	−1.42960	−0.50960	−0.04100	0.14930	0.23230	−0.03390	−0.39620	0.51500
5787.92	4.44	0.0	4.732	−0.78450	−0.69460	−0.08850	0.28170	0.61220	1.08170	1.35950	1.44730	−1.62860	−0.34790	0.08430	0.20330	0.23130	0.06660	−0.25960	0.55930
5824.45	4.44	0.5	4.705	−0.95150	−0.69700	−0.06460	0.32440	0.64470	1.09800	1.34930	1.44350	−1.80570	−0.33820	0.12800	0.23980	0.25710	0.09610	−0.23970	0.59420
5718.03	4.44	−0.5	4.785	−0.69890	−0.70920	−0.11910	0.24620	0.59040	1.08200	1.38680	1.47140	−1.53790	−0.37120	0.04620	0.17730	0.21680	0.03870	−0.28650	0.53520
5765.80	4.44	−1.0	4.748	−0.58150	−0.69110	−0.13560	0.21880	0.56260	1.04910	1.35270	1.43610	−1.41840	−0.37060	0.01940	0.14930	0.18870	0.01960	−0.29400	0.50690
5787.32	4.44	−2.0	4.732	−0.48830	−0.69910	−0.16960	0.18280	0.53630	1.02020	1.31860	1.40570	−1.32680	−0.39640	−0.01850	0.11930	0.16560	−0.01080	−0.32100	0.47790
5784.22	4.44	−3.0	4.735	−0.44810	−0.70850	−0.18920	0.16320	0.52400	1.00940	1.30620	1.39610	−1.28770	−0.41440	−0.03960	0.10440	0.15600	−0.02780	−0.33820	0.46410
5806.41	4.44	−4.0	4.718	−0.42430	−0.70840	−0.19780	0.15190	0.51230	0.99560	1.29050	1.38030	−1.26420	−0.41940	−0.05080	0.09250	0.14430	−0.03730	−0.34470	0.45220
6025.18	3.50	0.0	4.557	−0.65120	−0.57750	−0.04410	0.28120	0.58140	1.00060	1.22820	1.31580	−1.51480	−0.25890	0.09210	0.18060	0.18840	0.08460	−0.20280	0.53280
5988.06	3.50	−0.5	4.584	−0.57750	−0.58350	−0.07320	0.24900	0.55910	0.99250	1.23880	1.32330	−1.43830	−0.27770	0.05810	0.15520	0.17090	0.05920	−0.22540	0.50860
5907.99	3.50	−1.0	4.643	−0.54850	−0.61340	−0.10640	0.22340	0.54840	1.00290	1.27030	1.35510	−1.40580	−0.31300	0.02910	0.14000	0.16690	0.03450	−0.25650	0.49540
5961.94	3.50	−2.0	4.603	−0.46090	−0.60220	−0.13650	0.18370	0.51050	0.96200	1.23060	1.31350	−1.32050	−0.32360	−0.01030	0.10040	0.13010	0.00410	−0.27540	0.45620
5965.56	3.50	−3.0	4.601	−0.43190	−0.60880	−0.15100	0.16700	0.49750	0.95080	1.21940	1.30400	−1.29060	−0.33570	−0.02760	0.08580	0.11870	−0.01000	−0.28800	0.44230
5971.49	3.50	−4.0	4.596	−0.41640	−0.61290	−0.16090	0.15610	0.48770	0.94320	1.21470	1.29850	−1.27470	−0.34340	−0.03860	0.07550	0.10960	−0.01950	−0.29620	0.43230
6014.61	4.00	0.0	4.565	−0.63510	−0.58990	−0.05210	0.27640	0.57840	1.00220	1.23980	1.32370	−1.48810	−0.26890	0.08670	0.17710	0.18510	0.07870	−0.21020	0.52910
6038.71	4.00	−0.5	4.548	−0.52650	−0.58300	−0.07750	0.24160	0.54800	0.97380	1.21950	1.29990	−1.37710	−0.27850	0.05150	0.14520	0.15670	0.05300	−0.22700	0.49760
5958.44	4.00	−1.0	4.606	−0.49750	−0.61480	−0.11210	0.21450	0.53610	0.98300	1.24910	1.33020	−1.34490	−0.31560	0.02090	0.12870	0.15190	0.02690	−0.25960	0.48310
5954.96	4.00	−2.0	4.608	−0.43750	−0.63070	−0.14980	0.17680	0.50850	0.96150	1.23400	1.31640	−1.28550	−0.34630	−0.01860	0.09720	0.12860	−0.00600	−0.29090	0.45310
6032.46	4.00	−3.0	4.552	−0.38350	−0.61880	−0.16300	0.15260	0.47990	0.92310	1.18800	1.26910	−1.23210	−0.34640	−0.04130	0.06930	0.09810	−0.02370	−0.29780	0.42470
6023.76	4.00	−4.0	4.558	−0.37830	−0.62430	−0.17300	0.14000	0.46860	0.91710	1.18740	1.26780	−1.22630	−0.35410	−0.05410	0.05720	0.08810	−0.03440	−0.30700	0.41290
6020.75	4.50	0.0	4.561	−0.62240	−0.60530	−0.05810	0.27690	0.58070	1.00290	1.24360	1.32550	−1.46690	−0.28070	0.08660	0.17920	0.18680	0.07610	−0.21670	0.53100
5938.44	4.50	0.5	4.620	−0.84350	−0.64830	−0.04780	0.32120	0.62900	1.05840	1.29200	1.38240	−1.69580	−0.30130	0.12840	0.22750	0.23520	0.10120	−0.21670	0.57990
5968.38	4.50	−0.5	4.598	−0.54580	−0.61870	−0.08980	0.24110	0.55630	0.99720	1.26070	1.33920	−1.38610	−0.30410	0.04870	0.15120	0.16850	0.04730	−0.24340	0.50460
5961.60	4.50	−1.0	4.603	−0.48430	−0.62810	−0.11610	0.21340	0.53520	0.98260	1.25350	1.33230	−1.32270	−0.32400	0.01960	0.12800	0.15040	0.02390	−0.26450	0.48210
6064.09	4.50	−2.0	4.529	−0.37850	−0.62070	−0.15140	0.16540	0.48750	0.92170	1.18240	1.26070	−1.21880	−0.33990	−0.02760	0.07910	0.10230	−0.01400	−0.28860	0.43310
6024.94	4.50	−3.0	4.557	−0.36240	−0.64300	−0.17340	0.14780	0.47970	0.92350	1.19060	1.27150	−1.20220	−0.36560	−0.04740	0.06810	0.09880	−0.03140	−0.31050	0.42350
6037.83	4.50	−4.0	4.548	−0.34920	−0.64840	−0.18370	0.13650	0.46920	0.91320	1.18030	1.26130	−1.18910	−0.37440	−0.05880	0.05710	0.08880	−0.04160	−0.31940	0.41280
6432.73	4.00	0.0	4.273	−0.44620	−0.45690	−0.01340	0.26040	0.51590	0.86370	1.03890	1.11640	−1.30920	−0.17170	0.08240	0.12760	0.10220	0.08700	−0.15010	0.47320
6455.69	4.00	−0.5	4.258	−0.39190	−0.46130	−0.04240	0.22580	0.48510	0.83560	1.01710	1.09260	−1.25390	−0.18890	0.04730	0.09550	0.07330	0.05920	−0.17200	0.44140
6413.03	4.00	−1.0	4.286	−0.36430	−0.48480	−0.07670	0.19490	0.46490	0.83130	1.03060	1.10340	−1.22350	−0.21990	0.01440	0.07170	0.05800	0.03080	−0.20200	0.41910
6419.24	4.00	−2.0	4.282	−0.32650	−0.50660	−0.11630	0.15370	0.43180	0.80570	1.01380	1.08600	−1.18510	−0.25300	−0.02810	0.03530	0.02860	−0.00560	−0.23610	0.38400
6470.07	4.00	−3.0	4.248	−0.30140	−0.51070	−0.13440	0.12860	0.40500	0.77640	0.98300	1.05410	−1.15920	−0.26380	−0.05250	0.00860	0.00150	−0.02610	−0.25050	0.35720
6491.09	4.00	−4.0	4.234	−0.29550	−0.51950	−0.14770	0.11380	0.38990	0.76180	0.96910	1.04010	−1.15280	−0.27510	−0.06720	−0.00660	−0.01350	−0.03980	−0.26240	0.34210
6491.63	4.50	0.0	4.234	−0.40280	−0.45840	−0.01840	0.25180	0.50340	0.84300	1.01850	1.09080	−1.25470	−0.17330	0.07470	0.11630	0.08580	0.07990	−0.15270	0.46050
6503.68	4.50	−0.5	4.225	−0.34200	−0.47480	−0.05660	0.21110	0.47040	0.81610	1.00130	1.07120	−1.19170	−0.20250	0.03260	0.08080	0.05620	0.04510	−0.18400	0.42590
6435.89	4.50	−1.0	4.271	−0.32460	−0.50900	−0.09030	0.18460	0.45760	0.82040	1.02180	1.09230	−1.17110	−0.24010	0.00320	0.06380	0.04950	0.01840	−0.21670	0.41060
6500.28	4.50	−2.0	4.228	−0.28230	−0.52190	−0.13210	0.13260	0.40680	0.77100	0.97710	1.04490	−1.12910	−0.26750	−0.04840	0.01150	0.00010	−0.02500	−0.25060	0.35880
6499.46	4.50	−3.0	4.228	−0.26620	−0.54150	−0.15330	0.11380	0.39330	0.76150	0.97070	1.03950	−1.11160	−0.29040	−0.06830	−0.00380	−0.01110	−0.04360	−0.27080	0.34440
6507.77	4.50	−4.0	4.223	−0.26320	−0.55210	−0.16540	0.10200	0.38280	0.75240	0.96260	1.03170	−1.10820	−0.30260	−0.08030	−0.01480	−0.02100	−0.05520	−0.28230	0.33360
6907.57	4.50	0.0	3.964	−0.29660	−0.36800	−0.00300	0.22060	0.43030	0.70520	0.82860	0.89670	−1.15810	−0.11040	0.05350	0.05490	−0.00540	0.07110	−0.11930	0.39350
6986.84	4.50	−0.5	3.914	−0.26030	−0.37800	−0.03960	0.17480	0.38420	0.65680	0.78140	0.84700	−1.12200	−0.13320	0.00820	0.00850	−0.05110	0.03340	−0.14820	0.34710
7000.57	4.50	−3.0	3.906	−0.23350	−0.45660	−0.13960	0.07470	0.30170	0.59740	0.74610	0.80810	−1.08970	−0.22660	−0.09490	−0.08060	−0.12520	−0.05990	−0.24050	0.26070